

# **Deterministic Sorting by Electrical Properties and Morphology**

**Licentiate Thesis**

**Bao D. Ho**



**LUND**  
UNIVERSITY

Division of Solid State Physics and Nano Lund

Department of Physics

Lund University, Sweden

June 15, 2017

# Contents

<b>Abstract</b>	<b>iii</b>
<b>Preface and Acknowledgements</b>	<b>iv</b>
<b>Appended manuscripts</b>	<b>vi</b>
<b>1 INTRODUCTION</b>	<b>1</b>
<b>2 DETERMINISTIC LATERAL DISPLACEMENT</b>	<b>6</b>
2.1 Physics of fluid in motion . . . . .	6
2.2 Deterministic Lateral Displacement - basic principle . . . . .	8
<b>3 ELECTROKINETICS</b>	<b>12</b>
3.1 Electroosmotic flow and electrophoresis . . . . .	13
3.2 Dielectrophoretic force . . . . .	19
<b>4 METHODS AND EXPERIMENTS</b>	<b>21</b>
4.1 Simulation . . . . .	23
4.2 Device fabrication . . . . .	25
4.3 Experiments . . . . .	29

<b>5 SUMMARY OF MANUSCRIPTS</b>	<b>31</b>
5.1 Electrokinetic Deterministic Lateral Displacement . . . . .	31
5.2 Dielectrophoretic effect on red blood cells in deterministic lateral displacement . . . .	32
5.3 Sorting bacterial by chain length . . . . .	32
<b>6 CONCLUSIONS AND OUTLOOK</b>	<b>34</b>
<b>7 POPULAR SCIENCE SUMMARY</b>	<b>36</b>
<b>Bibliography</b>	<b>41</b>
<b>Manuscripts</b>	<b>44</b>

# Abstract

This Licentiate thesis focuses on fractionation of cells by size, electrical properties and morphology. More specifically, it started with Deterministic Lateral Displacement (DLD), a method capable of sorting cells based on size where mechanical irreversible interactions between a sufficiently large particle and obstacles in a microfluidic channel forces the particle to deviate from their smaller counterparts. This local deviation is amplified along the length of the channel, resulting in a lateral separation. It was then a natural idea to complement the mechanical interaction with an electrical interaction, making electrical properties another parameter for sorting in addition to size. Another idea is to exploit the difference in fluidic dynamic behaviors of different morphologies of cells and amplifying it using the principle of DLD to enable separation. The development of cell sorting methods from those two rationales has brought forth three manuscripts appended to this thesis. In the first manuscript, DC and AC fields were employed to tune an otherwise static DLD device and exploit surface charge as a marker for separation. The second manuscript demonstrated that an AC field can be used to orient the non-spherical red blood cells in a DLD device and in turn tuning their lateral displacement. Last but not least, the third manuscript provided a proof of principle of using DLD to sort bacteria by morphology, *viz.* their chain length, and presented a high throughput DLD device capable of sorting the large number of particles demanded by RNA analysis.

# Preface and Acknowledgements

It has been three years since my first visit to Lund for the interview of my current PhD position and also my first participation in LAPASO, the Label-free Particle Sorting consortium funded by the European Commission, even before I was officially admitted to the project. During the challenging but interesting journey thus far, I would like to thank my main supervisor, Jonas Tegenfeldt, who enrolled me into his team and introduced to me the field of cell separation. While giving me much freedom to try any ideas I could think of, he provided me with every necessary guidance and support during weekly group meetings and private meetings, networked me with experts in the fields he was not quite an expert on and gave me almost instant feedback on my work, manuscripts and even this thesis.

I would also like to thank Dr. Jason Beech, my other supervisor and also the person who has taught me a lot of practical knowledge and skills in microfluidics and soft lithography, cleanroom expertise, microscopy and so on. When things did not seem right in the lab, Jason would be the first person I turned to and he never refused to give a hand.

The work in this thesis would never be complete without collaboration and support from LAPASO principle investigators and fellows: Prof. Hywel Morgan, Dr. Daniel Spencer, Carlos Honrado from the University of Southampton; Prof. Birgitta Henriques Normark, Dr. Genevieve Garriss and Vitor Oliveira from Karolinska Institute; and other LAPASO partners and fellows who shared with me not only knowledge and experience but also fun time during dinners or afterworks

every time we had chance to meet.

I have also received tremendous help from my group mates: Trung, who is also my fellow Vietnamese friend and lunch companion, Kushagr, Stefan, Rebekah, and Oskar. I enjoy the discussion we have had about work and other interesting topics during “fikas” or afterworks.

I would also like to thank my colleagues at Solid State Physics and NanoLund, especially the members of the biogroup: Christelle, Heiner, Mercy, Damiano, Frida, Laura, Inga, Kalle; my office mates: Michael, Pyry, Steve, Enrique, and Reza. You have all made the Department of Physics my second home.

Last but not least, special thanks are to my parents and younger sister, who have given me unconditional love, support and encouragement, from very far away in Vietnam. My parents often laugh when I tell them I will win the Nobel prize in physics one day, but I know deep down they are always very proud of me.

# Appended manuscripts

Portions of the work described in this thesis have also appeared in the following manuscripts that have been prepared for publication:

## **I. Electrokinetic Deterministic Lateral Displacement**

Bao D. Ho, Carlos Honrado, Jason P. Beech, Daniel Spencer, Hywel Morgan, and Jonas O. Tegenfeldt

I designed and made the masters and the devices, performed the experiments, analyzed the data and did the simulation. I wrote the manuscript.

## **II. Dielectrophoretic effect on red blood cells in deterministic lateral displacement devices**

Bao D. Ho, Hasti Yavari, Stefan H. Holm, Si-Hoai-Trung Tran, Jason P. Beech, Jonas O. Tegenfeldt

I conceived the idea. I made the devices, performed the experiment, analyzed the data together with H. Yavari. I wrote most of the manuscript (section 2, half of section 3, 4, and 5).

## **III. Sorting bacteria by chain length**

Jason P. Beech\*, Bao D. Ho\*, Genevieve Garriss, Vitor Oliveira, Birgitta Henriques Normark, and Jonas O. Tegenfeldt

I planned the design together with J. Beech. I designed the devices. I made the devices, performed the experiments together with J. Beech, G. Garriss, and V. Oliveira. The bacteria distribution were counted and drawn by G. Garriss, V. Oliveira and J. Beech while the experiments and data analysis of the high throughput device were done by myself. J. Beech will be the main responsible author for writing and submitting the paper.

\*Authors contributed equally

# Chapter 1

## INTRODUCTION

“There’s Plenty of Room at the Bottom”

– *Richard Feynman.*

**H**UMANS have the tendency of miniaturizing their tools, making things smaller yet better and even cheaper. One excellent example is the computer. The replacement of bulky mechanical shafts and disks or electromagnetic relays and vacuum tubes by semiconductor components has helped miniaturizing a computer from a room-sized metal box to a cell phone in people’s pockets nowadays, with far better performance at much lower price. A rough analogy to microelectronics could be microfluidics: the former studies and makes use of solid state electronic circuits at micro and nano scale while the latter investigates and manipulates fluids in channels whose sizes are smaller than the width of a human hair. In fact, just like microelectronics, microfluidics has emerged as a field, encompassing a large number of research publications, enormous technological development and bringing about many start-up companies.

Microfluidics started in the late 70s with IBM ink jet printer nozzles [1] and Stanford University’s miniaturized gas chromatography [2]. The early works in microfluidics from the late 70s to the early 90s were closely related to microsystem

technology (MEMS); in fact, most of the early microfluidic products were made in silicon or glass, the familiar materials of MEMS industry. In this early stage, a large portion of the research focused on theory and modelling/simulation or technological aspects, like making of valves and pumps in silicon; applications were narrow and limited to flow sensors, ink jet printer nozzle arrays, micro dosing systems and microchemical analysis systems [3]. The next stage of microfluidics probably started with the introduction of soft lithography using polydimethylsiloxane (PDMS) [4] to fabricate devices, which have actually helped microfluidics depart from merely a branch of MEMS into a distinct field. The transparency of PDMS to visible and ultraviolet light and its compatibility to cells have made microfluidics more friendly to biological and medical applications and its “softness” has enabled the fabrication of flexible and easy to control pneumatic valves, mixers and pumps, broadening the capability of microfluidic devices. Besides silicon, glass, and PDMS, however, there are other choices for fabricating microfluidic devices, including thermoplastics (polystyrene, cyclic olefin copolymer, polymethyl methacrylate, and polycarbonate) and everyday materials (paper, wax, and cloth). The microfluidic community now has a wide range of materials to choose from to meet their specific requirements.

Current applications of microfluidics are even more diverse than the choices of materials used in fabricating them, mostly falling in the field of biology and medical research. Those applications can be found in rigorous reviews of the fields[5, 6]; as a quick reference, Figure 1.1 a) shows a word cloud listing the topics which make use of microfluidic concepts and technologies.

Almost forty years of research, development, and commercialization have brought microfluidics into today’s importance and visibility in our society. However, a large proportion of research in microfluidics is still in the engineering fields, as much as ten times that in biomedical and multidisciplinary fields [6] and a phenomenal “killer application”, like the personal computer or smart phone for microelectronics, has yet to arrive [5], [6]. Sackmann and colleagues, in their review paper

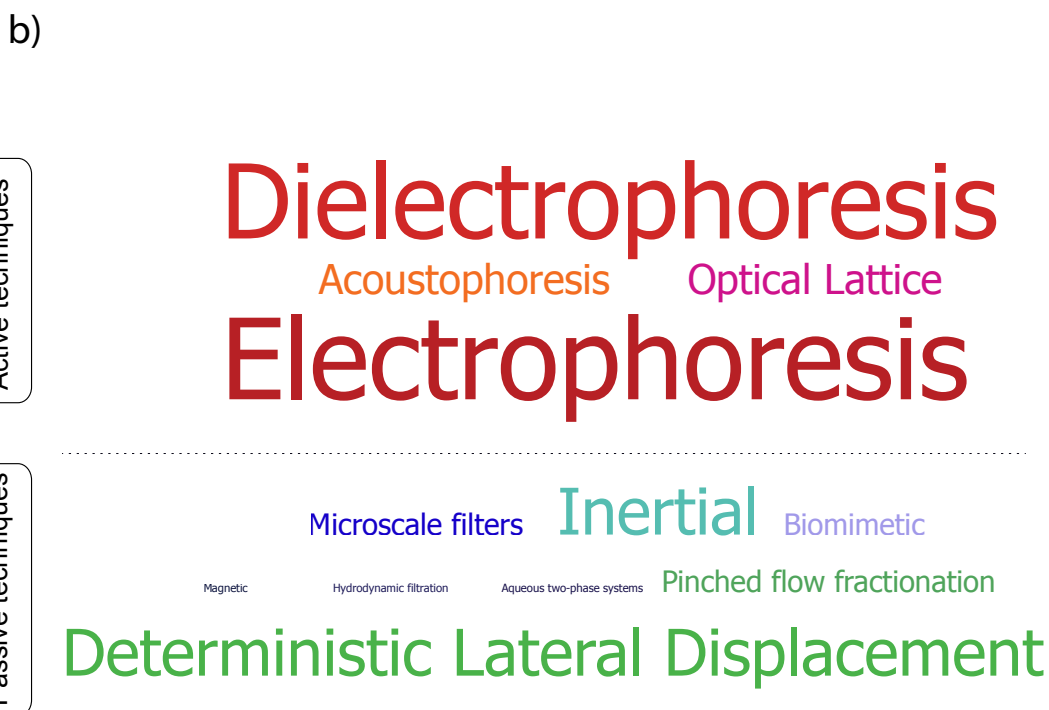
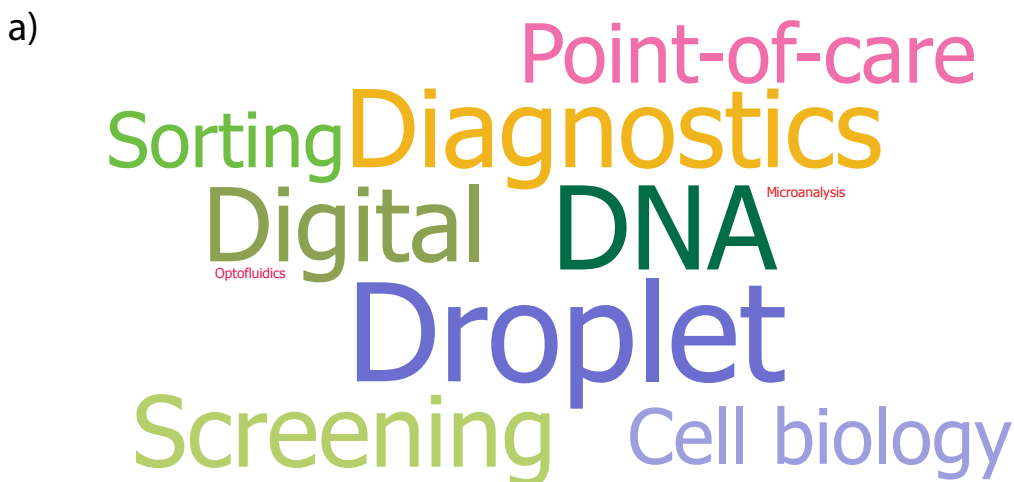


*Figure 1.1: a) A word cloud of applications of microfluidics, b) A word cloud of microfluidic label-free sorting techniques. In each figure, the font sizes are proportional to the logarithm of the number of publications of each application (in Figure a) or technique (in Figure b) found on Web of Science, on the date 20/05/2017. In Figure a), the result for “Sorting” for example, was determined by the key word: “TOPIC: (sorting) AND TOPIC: (microfluidics)”. In Figure b), the result for “Deterministic Lateral Displacement” for example, was determined by the key word string: “TOPIC: (Deterministic Lateral Displacement) AND TOPIC: (cell sorting)”. There are two exceptions: the key word “Microscale filters” did not yield relevant results, thus, its frequency was calculated as the median of other passive technique (for representation purpose only); the key word “Magnetic” may include results from magnetic tagging, thus, the topic “Label-free” was also included in the search string. The list here is not exhaustive and should not be used to compare relative importance of the listed applications or techniques. (Word cloud tool provided at <https://www.jasondavies.com/wordcloud/>).*

[6], made some well founded suggestions for successfully selecting and developing a topic in this field: offering fundamentally new capabilities instead of only improving upon existing methods, keeping the devices as simple as possible, fostering collaborations between physicists/engineers and biologists/medical experts, and finding the right problems. The work presented in this thesis falls into “Label-free sorting” category of microfluidics.

The term *Label-free sorting* is used to highlight the difference to traditional cell sorting techniques, which employ chemical labels or tags to identify cells of interest. Instead, label-free cell sorting exploits intrinsic physical properties to separate or enrich cells. Therefore, label-free sorting covers a wide range of different techniques targeting different physical properties of cells, including but not limited to size, shape, deformability, compressibility, density, dielectric properties, surface charge, *et cetera*. Techniques employed in label-free sorting can be split into two big groups. Active techniques require an applied force field, for instance electric field. Passive techniques do not demand such a field but instead rely on geometrical design. Readers may refer to the word cloud in Figure 1.1 b) to catch a glimpse of these techniques. Further details can be found in the rigorous review written by Daniel Gossett *et al.* [7] or the PhD thesis of Jason Beech [8].

Let us now examine the possibility of Label-free sorting being a mainstream practice in biomedical research, according the criteria proposed by Sackmann *et al.* [6]. First, considering fundamental novelty, it can be seen that while some techniques, for example microscale filters, improve upon the ideas which have been used to make their macro counterparts, other approaches, for instance Inertial Sorting or Deterministic Lateral Displacement, were completely new discoveries. When it comes to keeping the devices as simple as possible to lower the entrance threshold for biomedical technicians or end-users, most of the passive techniques can become good candidates since they usually need only a pressure generator, which can be as simple as a syringe. Active mechanisms often need some sort of apparatus to generate the required force field. Nevertheless, those apparatuses can be redesigned

and simplified to adapt to the local infrastructure. The third and fourth criterion, fostering collaborations between physicists/engineers and biologists/medical expert and finding the right problems to solve are open questions, since they are not dependent on the techniques but rather are determined by the needs and incentives of the experts. Nevertheless, as the most important purpose of label-free sorting is to avoid using chemical labels in cell sorting, this is potentially a real problem and collaborations should arise from a desire to find a solution. One such example is LAPASO, the Label-free Particle Sorting research project funded by the People Programme (Marie Curie Actions) of the European Union's Seventh Framework Programme, which brought together a multidisciplinary consortium of eight full partners and seven associate partners in Europe and Africa to solve current problems in the fields of bacteriology, parasitology, and rare cells sorting, using label-free methods. Further information can be found at its website: <http://lapaso.org>.

The work in this thesis is based on Deterministic Lateral Displacement, with the main focus on enhancing this technique by exploiting, besides size difference, electrical properties and shapes of the cells.

The thesis is structured as follows. After this Introduction chapter, Chapter 2 and Chapter 3 will present background on Deterministic Lateral Displacement and Electrokinetics. Chapter 4 will describe methods and practical details of the work and Chapter 5 summarizes the manuscripts intended for publications. The thesis ends with an appendix and the manuscripts.

# Chapter 2

## DETERMINISTIC LATERAL DISPLACEMENT

“Iron rusts from disuse; stagnant water loses its purity and in cold weather becomes frozen; even so does inaction sap the vigor of the mind”

– *Leonardo Da Vinci*

Understanding dynamics of fluid is important for this work since aqueous solutions were used to transport particles. This chapter starts with a brief review on fluid dynamics in Section 2.1 before introducing the Deterministic Lateral Displacement technique in Section 2.2.

### 2.1 Physics of fluid in motion

The Navier-Stokes equations are the fundamental equations of continuum fluid dynamics. The Navier-Stokes equations for incompressible flow, which is the case for most of microfluidic applications, consist of one vector equation describing momentum conservation and one scalar equation describing mass conservation [9, page 147]:

$$\rho \frac{D\mathbf{u}}{Dt} = \rho\mathbf{F} - \nabla p + \eta \nabla^2 \mathbf{u} \quad (2.1)$$

$$\nabla \cdot \mathbf{u} = 0 \quad (2.2)$$

Essentially, Equation 2.1 is Newton's second law applied to a unit volume of fluid: the term on the left hand side is the rate-of-change of momentum while the terms on the right hand side are the volumetric force and the surface forces. Since the density  $\rho$  is often uniform and known, there are four scalar unknowns ( $\mathbf{u}$  and  $p$ ) which can be solved using the four scalar equations in 2.1 and 2.2.

Equation 2.1 can be reduced further in microfluidics. The ratio between inertial effects and viscous effects is called the Reynolds number:

$$Re = \frac{\rho u D}{\eta}$$

Assuming density  $\rho = 1000 \frac{kg}{m^3}$ , viscosity  $\eta = 0.001 \frac{kg}{m.s}$ , average velocity  $u = 100 \frac{\mu m}{s}$ , and characteristic dimension  $D = 1 \mu m$ , a typical microfluidic device has the Reynolds number  $Re \simeq 10^{-3}$ , meaning that the inertial effects are very small in comparison with the viscous effects. In this case, the inertial term on the left hand side of Equation 2.1,  $\rho \frac{D\mathbf{u}}{Dt}$ , is negligible and the equation can be simplified into the *Stokes equation*:

$$\rho\mathbf{F} - \nabla p + \eta \nabla^2 \mathbf{u} = 0$$

The flow described by the Stokes equation is called *Stokes flow* or *creeping flow*, which is independent of time and thus can be time-reversible, meaning that fluidic

mixing is theoretically impossible (but diffusive mixing can still happen). A broader and less strict *low-Re* flow is called *laminar flow*, where the Reynolds number does not need to be very low (but should be less than 500) and the inertial term is still kept in Equation 2.1, only that it has relatively low influence in comparison with the viscous term.

## **2.2 Deterministic Lateral Displacement - basic principle**

In 2004 Lotien Richard Huang, James Sturm, Bob Austin, and colleagues demonstrated a novel method for sorting particles based on size [10]. Their paper, published in *Science*, now has been cited more than a thousand times. Despite being a seminal method, Deterministic Lateral Displacement (DLD) is surprisingly simple in its nature and in the way it can be implemented. Figure 2.1 describes the way DLD works from top view. A typical device is one centimeter long, one millimeter wide and ten micrometers deep, consisting of three parts: the inlet reservoirs on the left, the pillar array in the middle, and the outlet reservoirs on the right. The three inlet reservoirs are where silicone tubes are connected, allowing for loading sample and buffer liquid. The sample, consisting of a heterogeneous population of particles, is suspended in an aqueous medium and loaded into the middle inlet reservoir. The two inlet reservoirs on the sides are to create sheath flow, making sure the flow in the middle is straight along the device. When high throughput is needed, those buffer reservoirs can be removed (like in the high throughput device in manuscript 3). On the right hand side of the device, the number of outlet reservoirs needed is set by the number of populations being separated.

The Reynolds number of a DLD device is well below unity due to its small size; thus, the flow in the pillar array is a laminar flow. We refer to the line of pillars perpendicular to the flow direction a *row*; the next row along the flow direction is

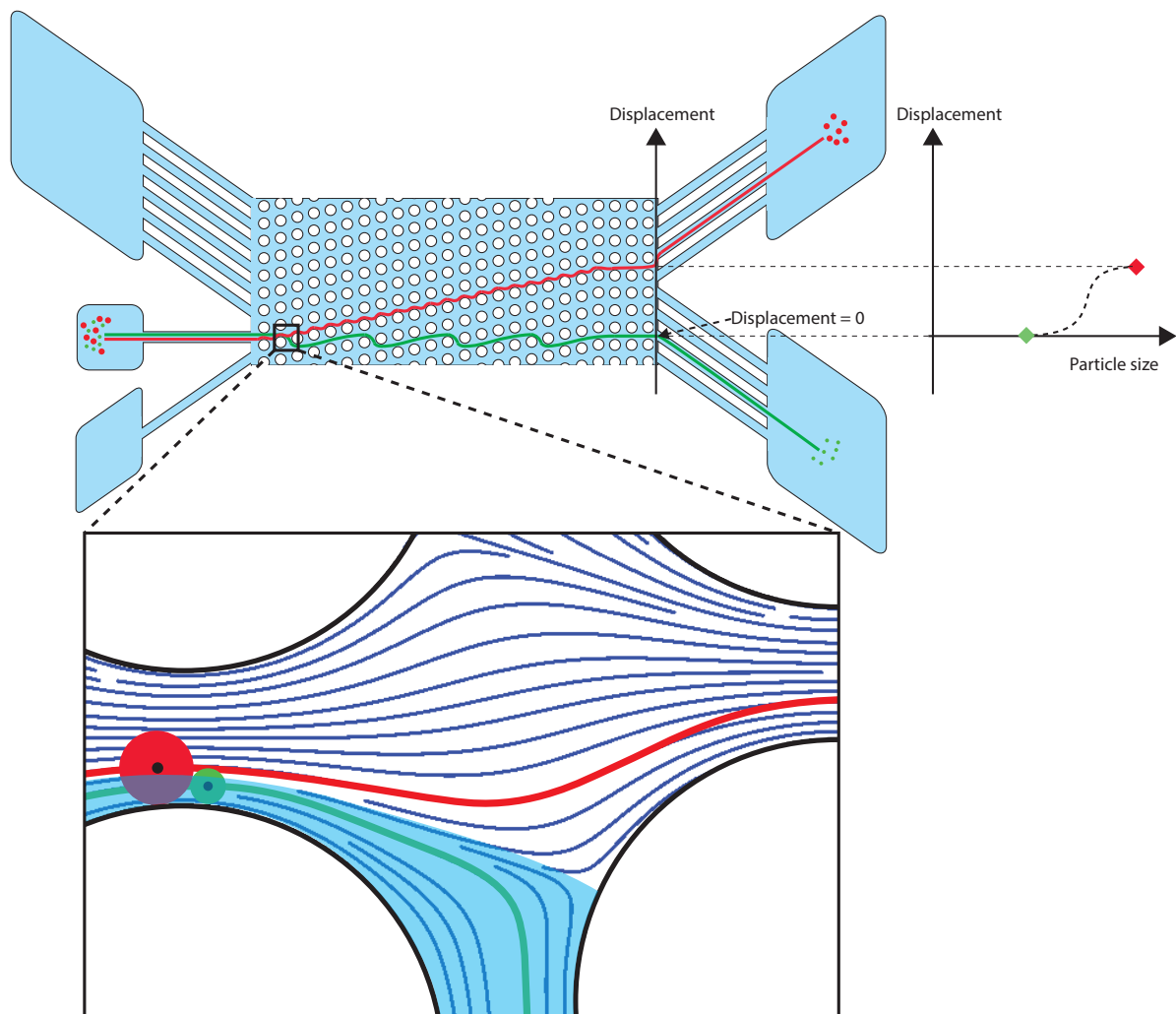


*Figure 2.1: Principle of Deterministic Lateral Displacement. The device, shown in the schematic at the top, is capable of sorting big (red) and small (green) particle in two populations. The inset at the bottom illustrates the mechanism. The size of the device and the number of pillars are not to scale.*

shifted up a distance *row shift* with respect to the previous row. The bifurcation of the flow as it encounters a pillar is crucial for the DLD. As can be seen at the bottom of Figure 2.1: a small stream of the flow goes around under the pillar while the rest keeps going straight above the pillar. A simple rule of thumb can now be applied to predict the behavior of the particles through the device. If the centre of the particle resides within the small stream (the green particle), the particle will also go around under the pillar while the bigger one (the red particle) will travel above the pillar (note that since the radius of the red particle is bigger than the small stream, it interacts sterically with every pillar it encounters and its centre of mass is pushed out of the small stream every time this happens). This separation is accumulated along the device causing different trajectories of the green and the red particles: one going zig-zag with zero net displacement and the other being displaced at an angle to the flow direction.

There is a *critical diameter* so that all particles smaller than that value move in the zig-zag mode while bigger ones are displaced. This critical diameter can be worked out assuming laminar flow with parabolic velocity profile between two posts of a row [11]. Beech and Tegenfeldt came up with a close-form analytical approximation for critical diameter [8, page 37]:

$$D_C = 1.2GN^{-0.5} \quad (2.3)$$

where  $D_C$  is the critical diameter,  $G$  is the gap between two posts in a row, and  $N$  is the period of the array (the pillars in the row  $N + 1$  has the same lateral positions as the pillars in the row 1). John Davis, in his PhD thesis [12], based on his experimental data, proposed an empirical formula for the critical diameter of a DLD, which has a similar form to the Equation 2.3, only anticipating a larger value of  $D_C$  for the same value of  $G$  and  $N$ .

$$D_C = 1.4GN^{-0.48} \quad (2.4)$$

Equation 2.3 and Equation 2.4 differ by around 20% – 25%, for typical device parameters. Equation 2.4 is normally used to estimate the critical diameter when designing DLD devices.

After more than ten years since its inception, DLD has found many applications in biomedicine, for example sorting WBC from RBC and plasma [13], [14], [15], separating circulating moving cells from blood [16], [17] or separating trypanosome from blood [18], [19].

From a technological perspective, DLD has been enhanced to sort particles based on other properties in addition to size, for example shape [18], [19], [20], deformability [20], [21], and electrical properties [22], [23].

The work presented in this thesis was driven by a need identified in an application (manuscript 3) and by a pure desire to develop the technology (manuscript 1 and 2). On the application side, the purpose is to collaborate with microbiologists to solve problems in bacteriology, whereas on the technical side, the focus is on either making the DLD device more flexible or adding new sorting parameters. However in the end, there is no real border between the two aspects.

# Chapter 3

## ELECTROKINETICS

In this chapter, the term *Electrokinetics* is an umbrella term to refer to three phenomena which can be used for transport (*-kinetics*) under application of an electric field (*Electro-*):

- Electroosmotic flow, which is the transport of ionic fluid using an electric field
- Electrophoresis, which is the transport of a charged particle using an electric field
- Dielectrophoresis, which is the transport of a dielectric particle using a non-uniform electric field

Electrophoresis is fundamentally caused by electroosmotic flow around a particle. Both are related to charges at the interfaces between an electrolyte and a solid wall, which can be the wall of a device or the surface of a particle. Dielectrophoresis is based on the polarization of a particle dictated by the dielectric property of the particle and a medium. Keen readers are advised to consult the book: “*AC electrokinetics: colloid and nanoparticles*” by Morgan and Green [24] for more details.

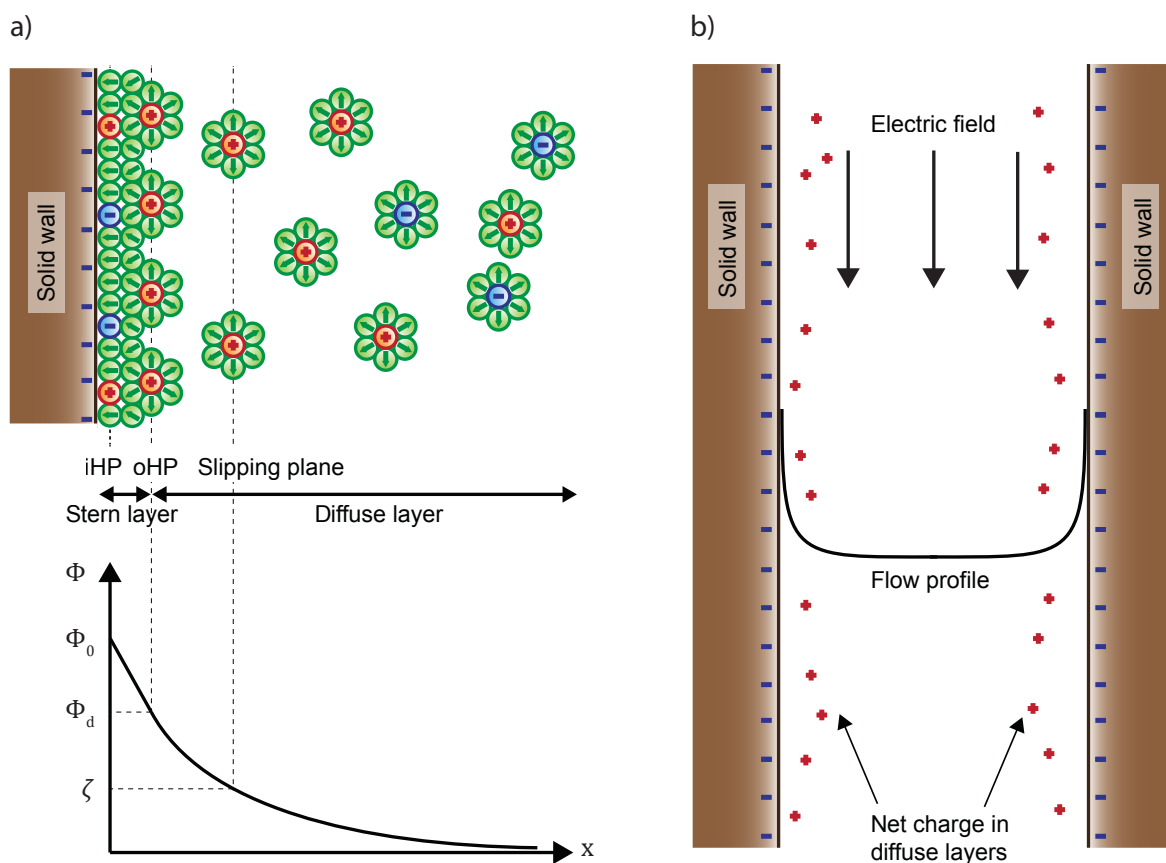


Figure 3.1: a) Structure of double layer; b) Mechanism of electroosmotic flow

### 3.1 Electroosmotic flow and electrophoresis

#### Electroosmotic flow

It was known for more than two hundred years that a voltage can transport an electrolyte in a channel with charged walls [25]. This phenomenon can be explained by the theory of *electrical double layer*. Several models have been developed to explain the electrical double layer. The currently commonly used model was proposed by Bockris *et al.* [26]. According to this model, when a charged solid wall is embedded into an electrolyte, the ions of opposite polarity from the solution are attracted to the surface of the object to screen the surface charge. As illustrated in Figure 3.1 a), the first region from the object surface consists of solvent dipoles, usually water molecules, and ions of both polarities. Farther from the surface is a region of hydrated ions of opposite polarity and finally the diffuse layer where the ions “diffuse” into bulk electrolyte, or in other words, the charge density reduces

exponentially to zero, reaching neutrality. The plane passing through the loci of bounded dipoles and ions is called *the inner Helmholtz plane* and the plane passing through the loci of hydrated ions is named *the outer Helmholtz plane*. *The Stern layer* residing between the object surface and the outer Helmholtz plane consists of molecules and ions bounded to the object surface. *The diffuse layer* is located where the hydrated ions can move relative to the object surface. The term *double layer* refers to the Stern layer and the diffuse layer. The characteristic thickness of the double layer is the *Debye length*, written as  $\lambda_D$  or  $\kappa^{-1}$ , defined as the distance at which the potential falls to  $1/e$  of its maximum value. For a symmetric monovalent electrolyte like *KCl*, the Debye length can be calculated as:

$$\lambda_D = \sqrt{\frac{\varepsilon k_B T}{2q^2 n_0}}$$

where  $\varepsilon$  is the permittivity of the solution,  $k_B$  is the Boltzmann constant,  $T$  is the absolute temperature,  $q$  is the elementary charge, and  $n_0$  is the number density of the ions in the bulk. For a 1M KCl solution at room temperature:  $\varepsilon = 80 \times 8.85 \times 10^{-12} \text{ F/m}$ ,  $k_B = 1.38 \times 10^{-23} \text{ J/K}$ ,  $T = 293 \text{ K}$ ,  $q = 1.60 \times 10^{-19} \text{ C}$ ,  $n_0 = 6.02 \times 10^{26} \text{ m}^{-3}$ , the Debye length is:  $\lambda_D = 0.305 \text{ nm}$ . For a 1mM KCl solution at room temperature ( $\sigma \simeq 15 \text{ mS/m}$ ),  $\lambda_D = 9.6 \text{ nm}$ .

The concept of electrical double layer can be used to explain electroosmotic flow. Due to the structure of the electrical double layer, for the case in Figure 3.1 a), the potential drops linearly from the inner Helmholtz plane ( $\phi_0$ ) to the outer Helmholtz plane ( $\phi_d$ ) and exponentially from the outer Helmholtz plane into the bulk electrolyte. The charge density also decreases exponentially from the outer Helmholtz plane into the bulk electrolyte. Thus there is a net charge in the diffuse layer. If an electric field is applied tangential to the wall, as illustrated in Figure 3.1 b), at some certain plane in the diffuse layer, called the *slipping plane*, the counter charges will move, dragging the fluid with them to form a plug-like flow profile. The potential at the slipping plane is called the *zeta potential*

( $\zeta$  - potential), which can be calculated from measured electroosmotic flow velocity, using the Helmholtz– Smoluchowski equation:

$$u_{EOF} = -\frac{\varepsilon\zeta}{\eta}E_t \quad (3.1)$$

Where  $\varepsilon$  is the permittivity of the fluid,  $\eta$  is the viscosity of the fluid, and  $E_t$  is the electric field component tangential to the wall.

It is convenient to define the *electroosmotic mobility*, which is the ratio between the electroosmotic velocity and the (tangential) electric field:

$$\mu_{EOF} = \frac{u_{EOF}}{E_t} = -\frac{\varepsilon\zeta}{\eta}$$

## **Electrophoresis**

The electrical double layer also forms when a charged particle is in contact with an electrolyte. In this situation, the relation between the size of the particle and the thickness of the double layer needs to be considered. If the particle is roughly one micrometer or bigger, which is much larger than the thickness of the double layer (several nanometers), similar arguments as with electroosmotic flow can be used and the electrophoretic velocity can be calculated as [27][28]:

$$u_{EP} = \frac{\varepsilon\zeta}{\eta}E \quad (3.2)$$

This equation is very similar to the equation of electroosmotic flow (3.1), only with the difference in sign. It is because in both cases, the physical chemistry effects are the same, only that Equation 3.1 expresses fluid velocity with respect to a wall while Equation 3.2 calculates the particle (wall) velocity with respect to the fluid, hence the sign difference.

It is, again, convenient to define the *electrophoretic mobility*, which is the ratio between the electrophoretic velocity and the electric field:

$$\mu_{EP} = \frac{u_{EP}}{E} = \frac{\varepsilon\zeta_P}{\eta}$$

When the particle is on the order of nanometers, which is in the limit of a thick double layer, a different equation for electrophoresis should be used [28]:

$$u_{EP} = \frac{2\varepsilon\zeta_P}{3\eta}E \tag{3.3}$$

Which is two thirds less than in the case of thin double layer.

### **Measurement of phase lag between electroosmotic flow and electric field**

The normal situation in electrokinetics, which is also the case in capillary electrophoresis, is that electroosmotic flow and electrophoresis take place simultaneously. Conceivably, they must have different response time because the inertia of the volume of a fluid is much larger than that of a single particle. If there is any phase lag between the movement of a bead when applying, for example, an AC sinusoidal field, it would be attributed to the slower response of electroosmotic flow.

To investigate this matter, electrokinetic experiments were performed in a DLD device with carboxylate-modified beads of  $2\ \mu\text{m}$  diameter suspended in a KCl solution having the conductivity of 25 mS/m. The high intensity LED lamp used to expose the fluorescent beads was synchronised with the AC electric signal used to drive the beads. The electrical setup performing this task is shown in Figure 3.2.

The output sinusoidal signal from a function generator (15 MHz function/arbitrary waveform generator, model 33120A, Hewlett Packard, Palo Alto, CA, USA) was amplified 100 times by a Bipolar operational power supply/amplifier (BOP 1000M,

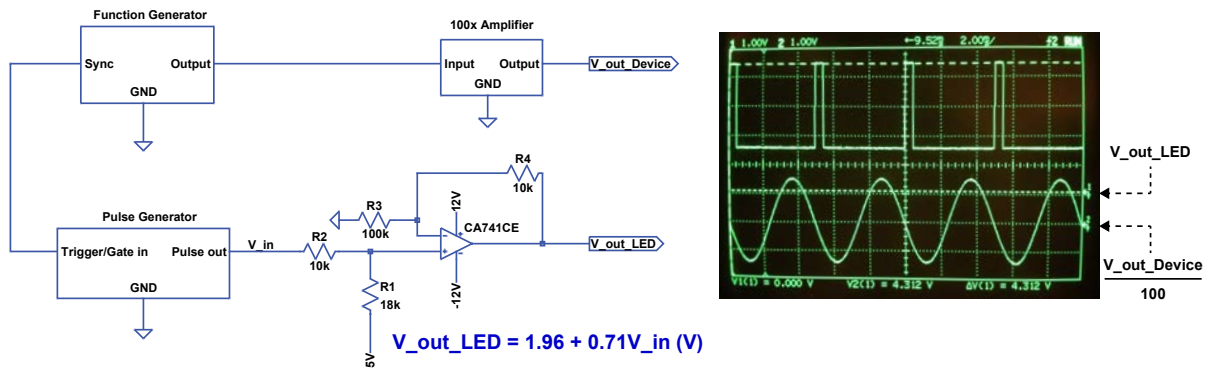
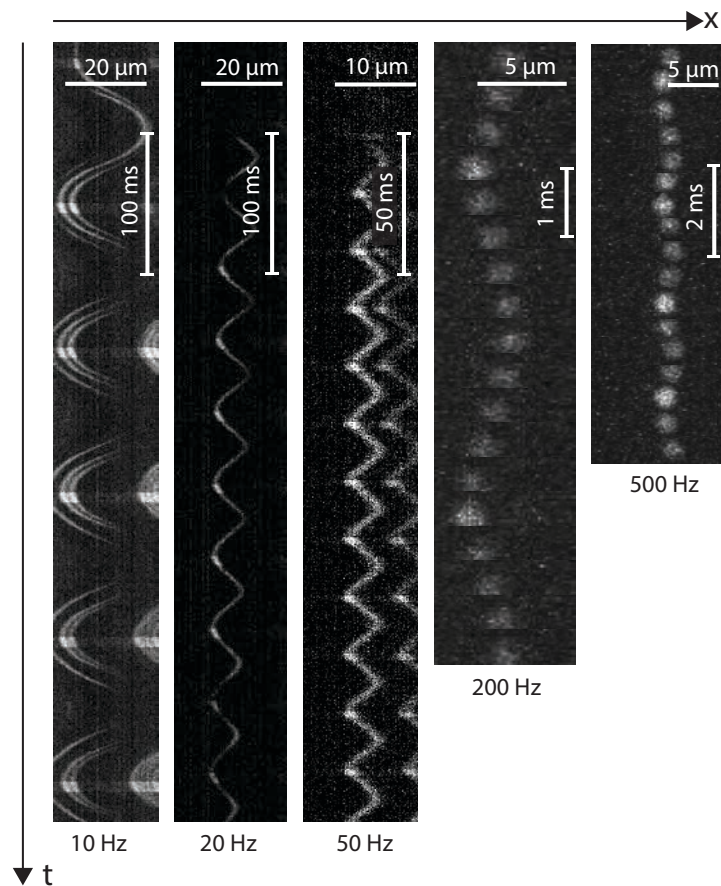


Figure 3.2: Schematic of electrical setup (left) and oscilloscope screen showing the synchronized voltages fed to LED and to device (right)

Kepeco, Flushing, NY, USA) whose output was applied across the device. The sinusoidal signal from the function generator was synchronized with a square signal from a pulse generator (TGP110 10MHz Pulse generator, Thurlby Thandar). The square signal had adjustable duty cycle, capable of providing a very short pulse to the LED. An op-amp voltage adder circuit was used to raise the space period of the square signal to a level above zero, making the beads visible even during the space period. As a result, an observer would see the beads lit for a short period of time at the beginning of the sinusoidal signal and dimmed during rest. The phase lag between the mechanical oscillation of the beads and the sinusoidal signal, if it exists, can be pinpointed by the phase lag between the lit period and the starting point of each oscillation.

The results are shown in Figure 3.3, which demonstrates that up to 200 Hz, the beads lit up at the beginning of their oscillation cycles, there was no visible lagging between the beads oscillation and the electric field. Since there is no electroosmotic suppressor in the medium, electroosmotic flow will dominate over electrophoresis [29, 30]; thus, the results suggest that the electroosmotic flow was not lagging behind the electric field. This conclusion may also apply at 500 Hz, although the small amplitude of the oscillation at this frequency made it difficult to tell.

In conclusion, electroosmotic flow is fast enough to keep pace with electric field at frequencies up to 200 Hz.



*Figure 3.3: Kymographs showing position of beads as a function of time. The videos were taken at 2100 frames per second. The spatial and temporal scales are different for each graph.*

**Similitude between electroosmotic flow and electric field** It has been reported in literature [31, 32] that there is a similitude between electroosmotic flow and electric field. It means that everywhere in a microfluidic channel the electroosmotic velocity vector and the electric field vector are parallel and their magnitudes differ by a constant ratio:

$$\mathbf{u}_{EOF} = -\frac{\varepsilon\zeta}{\eta}\mathbf{E}$$

Further more, if we assume that particles are much smaller than the channel, the electrophoretic velocity is also parallel and proportional to the electric field:

$$\mathbf{u}_{EP} = \frac{\varepsilon\zeta_P}{\eta}\mathbf{E}$$

If the channel wall is homogeneous, there would be a similitude between the beads velocity ( $\mathbf{u} = \mathbf{u}_{EOF} + \mathbf{u}_{EP}$ ) and electric field, meaning that everywhere in the channel, the beads velocity due to electroosmosis and electrophoresis would be parallel and proportional to electric field, which reduces the problem of solving velocity to solving electric field. This applies to DC and low frequency AC, up to at least 200 Hz as has been shown earlier.

## 3.2 Dielectrophoretic force

The DEP force,  $\mathbf{F}_{DEP}$ , on a spherical particle of radius  $a$  in a non-uniform electric field  $\mathbf{E}$  can be calculated as:

$$\mathbf{F}_{DEP} = \pi\varepsilon_m a^3 Re \left( \frac{\tilde{\varepsilon}_p - \tilde{\varepsilon}_m}{\tilde{\varepsilon}_p + 2\tilde{\varepsilon}_m} \right) \nabla |\mathbf{E}|^2 \quad (3.4)$$

where  $\tilde{\epsilon}_m, \tilde{\epsilon}_p$  are the complex permittivities of the particle and the suspending medium, defined as:  $\tilde{\epsilon} = \epsilon - i\sigma/\omega$ . Here  $\epsilon$  is the permittivity of the particle or the medium,  $\sigma$  is the conductivity of the particle or the medium and  $\omega$  is the angular frequency of the electric field. One should note that Eq. 3.4 applies well only when the magnitude of the electric field does not vary significantly across the dimensions of the particle [24, page 51].

# Chapter 4

## METHODS AND EXPERIMENTS

“If you optimize everything, you will always be unhappy.”

– *Donald Knuth.*

**T**HIS chapter describes how the research is done. The methodology is summarized in Figure 4.1. To start with, the ideas come from either *a technological-driven approach* (literature and our previous work) or *an application-driven approach* (biological or medical needs). To probe the feasibility of the ideas, ideally a modelling or simulation step is performed (see section 4.1), but in some cases they can be skipped if the idea is simple. The next step, fabricating microfluidic devices includes several sub steps: designing and making photolithographic masks, making the mold and finally casting and bonding devices. The details can be found in section 4.2. The newly fabricated devices will be loaded with polystyrene or biological particles and the particles will be separated in planned, designed experiments under a microscope (see section 4.3). In the next step, experimental data, often high frame rate microscopic videos, will be processed, analysed, and compared with simulation results (see section 4.3). The information coming out from the analysis step will be used to judge whether the research has yielded the outcome envisioned when started or if the starting ideas need to be refined or improved.

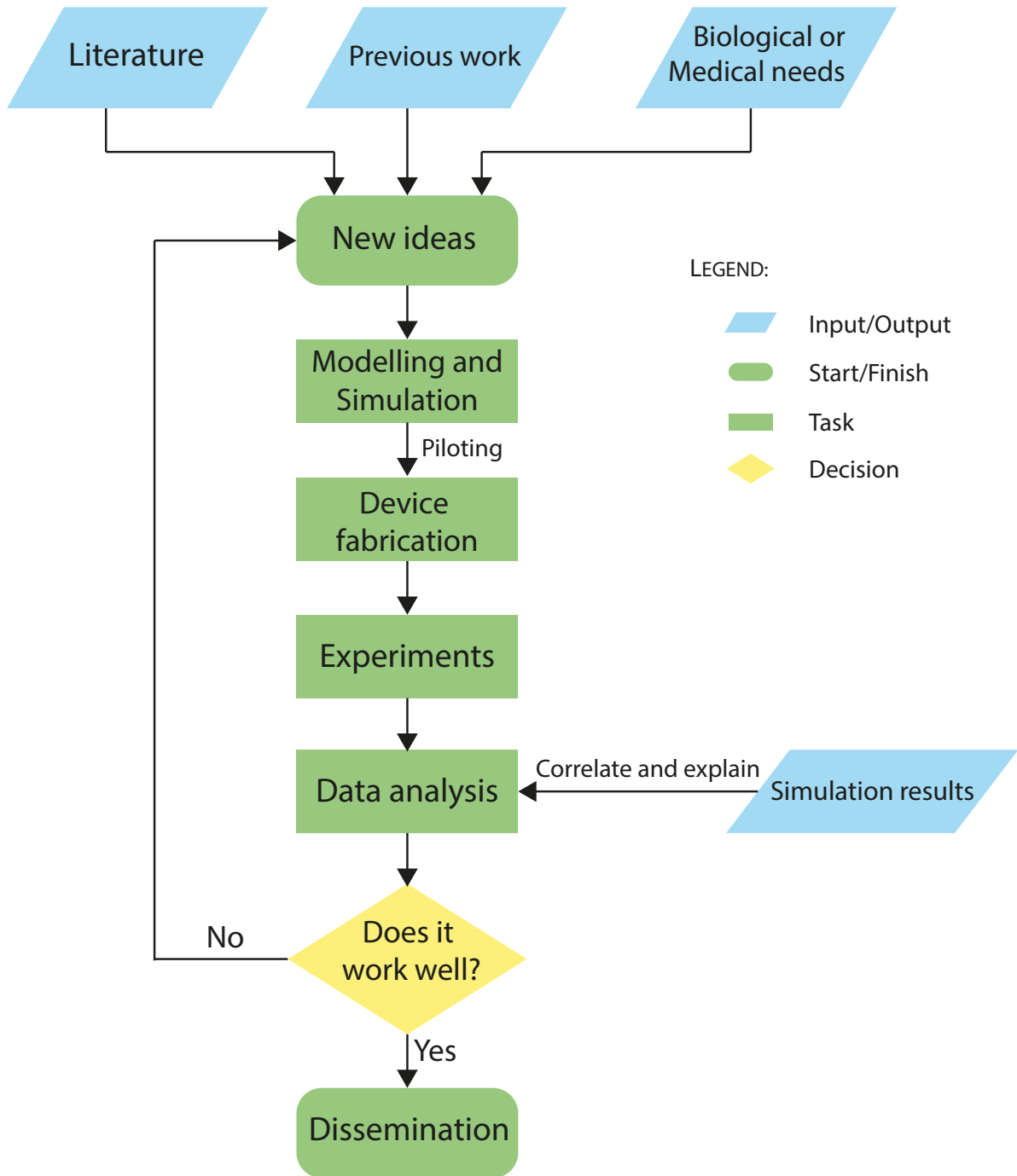


Figure 4.1: Methodology flow chart

## 4.1 Simulation

When the geometry is complicated or when the mathematics is too complex to produce an analytical solution, especially when many physical mechanisms are involved, a numerical simulation based on differential equations and proper boundary conditions provides a rather direct, engineering way to look at the problems at hand. All the simulations in this work were built using COMSOL Multiphysics. The physics used are summarized below and more details can be found in Table 4.1.

*i. Laminar flow* is used for calculating the velocity profile of the fluid in the devices. Since the Reynolds number of microfluidic devices is well below unity, the inertial component can be neglected. Also, since the fluid velocity is well below the speed of sound, the flow is assumed incompressible. The wall boundary condition can be non-slip (pressure driven flow) or slip boundary condition (electroosmotic flow).

*ii. Wall distance* is useful when calculating the distance from the centre of mass of a particle to a wall to apply a wall force. It is described using an *Eikonal equation*.

*iii. Electric current* provides solution to electric field in the device, which will be used later as an input to calculate electroosmotic flow and dielectrophoretic force. In this work, it is assumed that there is no current source or external current density.

*vi. Particle tracing for fluid flow* provides a computationally reasonable way to simulate dynamics of the particles in a DLD device under the combined action of pressure driven flow, electroosmotic flow, electrophoresis and dielectrophoresis.

Physics	Differential equations/Boundary conditions	Meaning
Laminar flow	$0 = \nabla \cdot [-p\mathbf{I} + \mu(\nabla\mathbf{u} + (\nabla\mathbf{u})^T)] + \mathbf{F}$	Inertial term neglected (left hand side), surface forces and body forces adds up to zero (RHS).
	$\rho\nabla \cdot \mathbf{u} = 0$	Incompressible flow
	$\mathbf{u} = 0 \big _{walls}$	No-slip boundary condition
Wall distance	$\mathbf{u} = \mu_{EO}\mathbf{E}_t \big _{walls}$	Electroosmotic flow boundary condition
	$p = p_0 \big _{inlet}, p = 0 \big _{outlet}$	Pressure at the inlet and outlet of the device
	$ \nabla D  = 1$	The norm of the gradient of wall distance is unity
	$D = 0 \big _{wall}$	Wall distance is zero for the points on the wall
Electric current	$\nabla \cdot \mathbf{J} = 0$	Continuity equation of current
	$\mathbf{J} = \sigma\mathbf{E}$	Ohm's law in steady state
	$\mathbf{J} = (\sigma + j\omega\epsilon_0\epsilon_r)\mathbf{E}$	Ohm's law in frequency domain
	$\mathbf{J} = (\sigma + \epsilon\epsilon_r\frac{\partial}{\partial t})\mathbf{E}$	Ohm's law in transient state
	$\mathbf{E} = -\nabla V$	Definition of electric potential
	$V = V_0 \big _{inlet}, V = 0 \big _{outlet}$	Voltage at the inlet and outlet of the device
Particle tracing for fluid flow	$\frac{d}{dt}(m_p\mathbf{v}) = \mathbf{F}_t$	Newton's second law
	$\mathbf{F}_D = \frac{1}{\tau_p}m_p(\mathbf{u} - \mathbf{v})$	Drag force, Stokes form used for laminar flow
	$\tau_p = \frac{\rho_p d_p^2}{18\mu}$	Particle velocity response time for spherical particles in a laminar flow
Wall repulsive force	$\mathbf{F}_w = F_{w0} \times step(D - r_p) \times (-\mathbf{D}_{dir})$	Wall repulsive force
	$\mathbf{F}_{DEP} = 2\pi r_p^3 \epsilon_m Re \{f_{CM}\} \nabla  \mathbf{E}_{rms} ^2$	Dielectrophoresis force
	$f_{CM} = \frac{\epsilon_p^* - \epsilon_m^*}{\epsilon_p^* + 2\epsilon_m^*}$ $\epsilon^* = \epsilon - j\frac{\sigma}{\omega}$	The Clausius-Mosotti factor Complex permittivity

Table 4.1: Physics used in simulation

## 4.2 Device fabrication

The devices were made from a silicon-based organic polymer called *Polydimethylsiloxane* (PDMS), which has several advantages for manipulating biological particles using microfluidics: it is transparent, non-toxic (to the extent that it can be used in food and shampoo), impermeable by water but permeable by air and other gases. The main drawback of PDMS is that it is hydrophobic and thus wetting a PDMS device requires surface oxidation by oxygen plasma treatment. The making of a PDMS device, which has been a standard technique and was described in detail in the literature [4], includes three steps:

*i.* Drawing of the device's features in an electronic file. The software L-Edit was used for this task.

*ii.* Getting the mask fabricated by a mask manufacturing company (often Delta-Mask) and performing soft UV lithography in Lund NanoLab to make a mold for patterning PDMS. The mold is essentially a layer of SU8 on a silicon wafer which has the negative landscape corresponding to the shapes of the features on the device. An antisticking step with tridecafluoro-(1,1,2,2)-tetrahydrooctyl-trichlorosilane (F13-TCS) (Sigma Aldrich, Saint Louis, MO, USA) is needed to promote the peeling off of PDMS later.

*iii.* Pouring liquid PDMS on the mold and letting it cure at  $80^{\circ}\text{C}$  for an hour. The PDMS layer is then peeled off the mold, trimmed, perforated with access holes, treated with oxygen plasma, bonded on a glass slide, and connected to silicone tubes for pressure control.

A master and a device are shown in Figure 4.2.

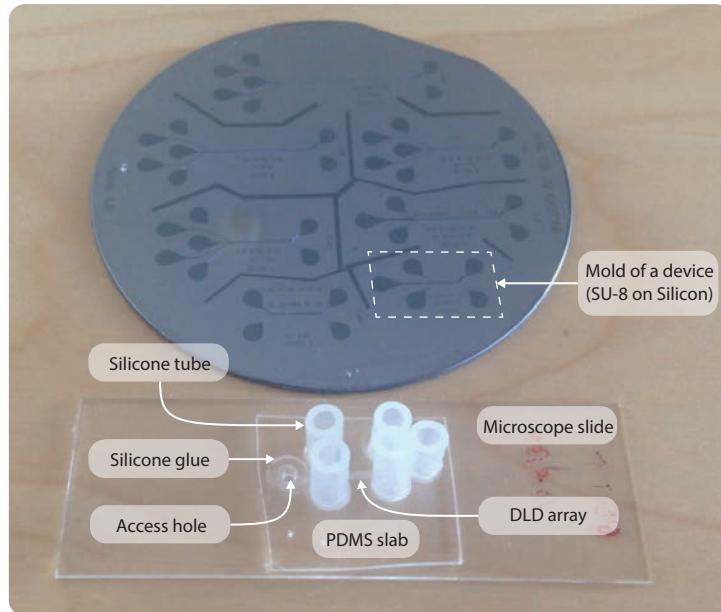


Figure 4.2: A master made with patterned SU-8 layer on a silicon wafer and a bonded PDMS device.

### Automating drawing devices using L-Edit

Although details can be more complicated, a typical DLD device is illustrated in Figure 4.3a. The green areas are hollow space where liquid can flow while the white areas are PDMS obstacles or walls. A typical device consists of input and output reservoirs, an array of posts (a.k.a. pillars or bumpers) where the separation takes place, and channels connecting the array and the reservoirs. Within the array, the posts are arranged inclined with the overall flow direction, facilitating deterministic displacement (more details can be found in Chapter 2). Edge correction [33] is implemented to minimize wall effects and straight ends are positioned between the array and the connecting channels to ensure the particles go straight when they enter the array.

L-Edit allows users to draw basic shapes like rectangles, circles, polygons, *etc.* whose dimensions can be specified precisely and provides functions to transform the shapes, for example making an array of a shape or subtract a shape from one another. A more complex geometry, for example a DLD array, can be constructed from basic shapes via a hierarchical approach, the *cells* mechanism, in

which a cell at higher hierarchical level can be built by populating it with instances of cells at lower level, making it easy to modify or reuse a design. It also supports programmable drawing mode via *T-cell* (Template cell), which is a program written in the C language, allowing users to draw shapes of parameterized size or quantity using internal functions of L-Edit. Both the GUI and the programmable interface have their own advantages. The GUI provides flexible drawing and positioning of shapes in specific cases when programming is impossible whereas the programmable interface makes it possible to design and place features in a parametric and batching manner. The two approaches can be combined to optimize the designing process.

The process of designing the devices is described in the diagram of Figure 4.3b. Some minor details are not presented to keep the picture simple. All the cells painted green are T-cells and so their names start with the verb “generate” to reflect the fact that they are small programs, generating cells defined by user’s input parameters. The cells painted orange are cells created using the GUI and contain the top level geometries. The reservoirs can be drawn either by coding or by the GUI, depending on the specific situation. The design task starts with creating posts (*Generate posts*) and then arranging posts into either a straight end or a period with precise space between posts and with edge correction near the wall (*Generate straight end* and *Generate period*). The straight ends and the periods are then combined into the array (*Generate array*) and the connecting channels are also generated (*Generate In/Outlet channel*). The reservoirs have some parts which can be programmed, like arranging supported posts with equal space to prevent PDMS from collapsing, but also some parts can be done easier with GUI. A device is then constructed by combining the array, the connecting channels and the reservoirs and finally, a wafer is populated by arranging as many as possible devices on it. The final task of arranging a DLD array, reservoirs and connecting channels into a device or several devices on a mask requires some specific alignments which are more easily done with the GUI than with coding. One side note

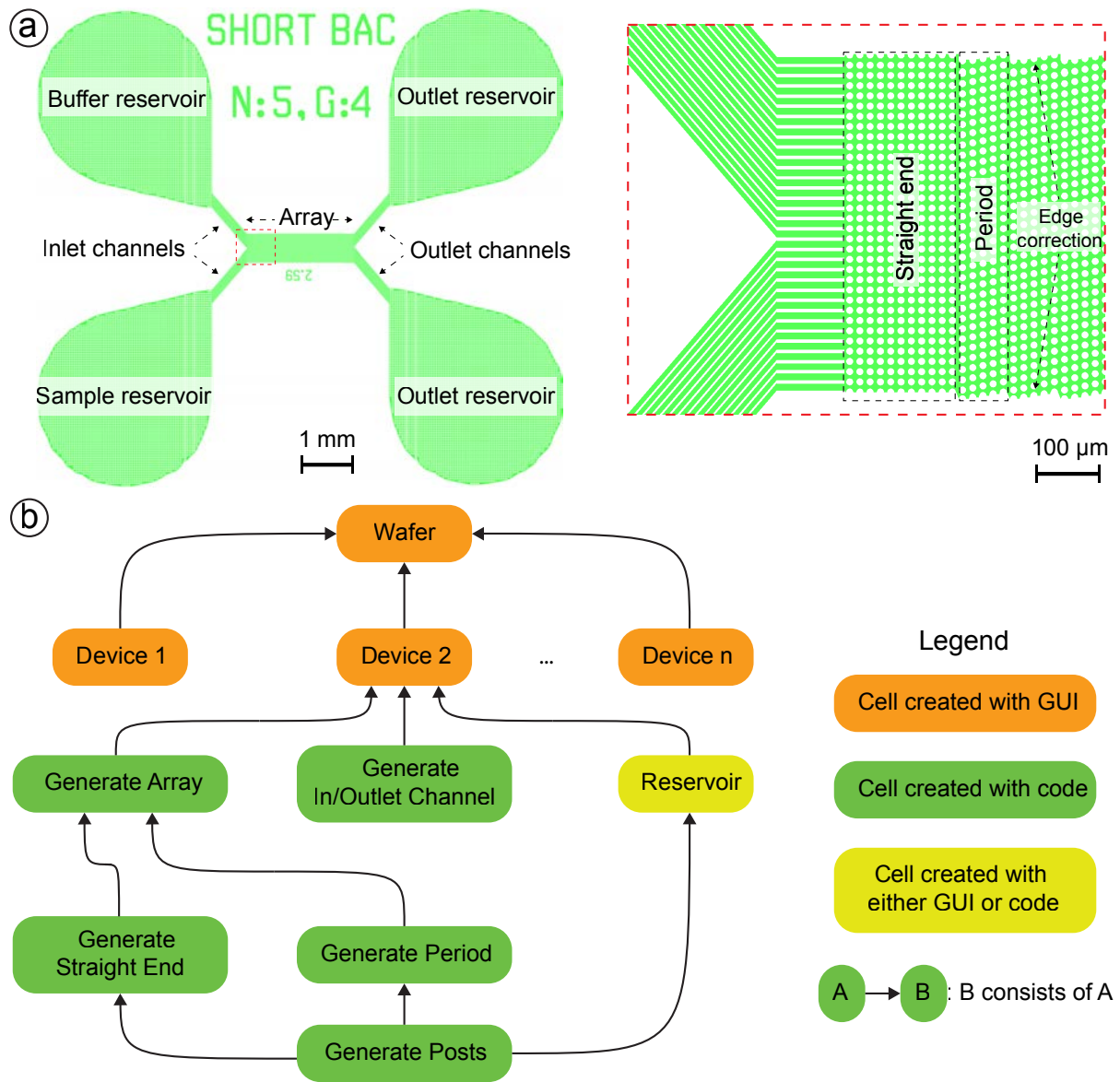
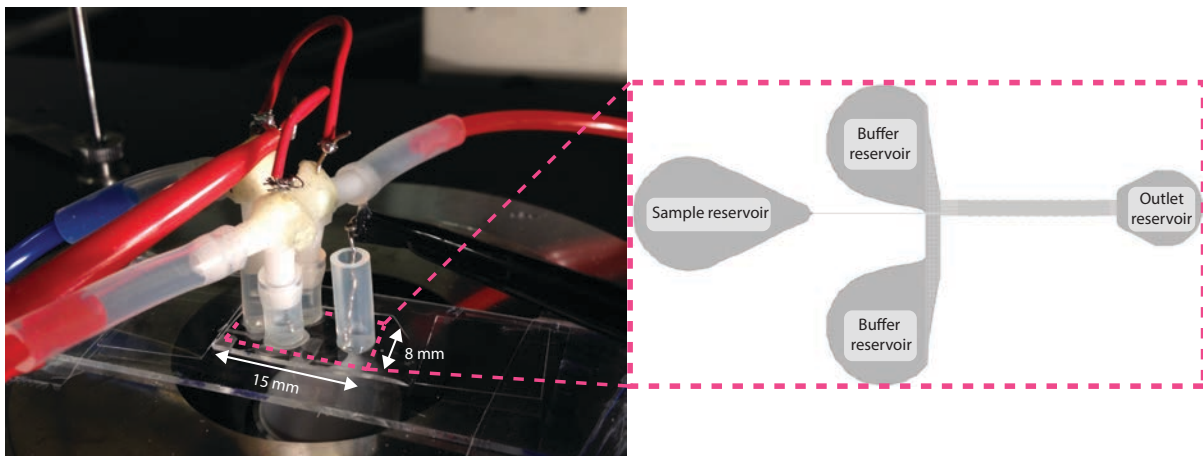


Figure 4.3: a) A typical DLD device, b) The design is structured in a hierarchical order, using cells

is that although the procedure was described in a bottom up manner, when all the modules (T-cells) have been prepared, the designing process is carried out top down. For example, generating an array is performed by solely calling the corresponding T-cell with its own parameters without paying any attention to the T-cells at lower levels (*Generate straight end*, *Generate period* or *Generate posts*), which makes the designing task easy and convenient.

As an example, the source code for the T-cell *Generate array* is presented in Appendix 7.

### 4.3 Experiments



*Figure 4.4: Schematic overview of a DLD device connected to tubing and electrical wiring along with an overviewing of the layout of the reservoirs.*

A typical experimental setup is shown in Figure 4.4. A pressure gradient was created by letting the outlet reservoir be open to the ambient air while connecting inlet reservoirs to an over pressure controller or a syringe pump. The setup presented here use a *MFC5 – 4C* pressure controller (Fluigent, Paris, France), tubes and T-connectors to interface with the silicone tubes of the device. An alternative way, which is not shown in the picture, could be connecting the inlet reservoir to atmospheric pressure while connecting the outlet reservoirs to a vacuum pump or a syringe run in reverse. To bias the device with a voltage, as required by the ex-

periments of manuscript 1 and 2, holes were drilled through the T-connectors and platinum electrodes were pushed through the holes, glued and embedded into the liquid in the silicone tubes of the device.

To generate DC or AC fields, a function generator (15 MHz function/arbitrary waveform generator, model 33120A, Hewlett Packard, Palo Alto, CA, USA) was used and signals were amplified 100 times by a Bipolar operational power supply/amplifier (BOP 1000M, Kepco, Flushing, NY, USA) to give a maximum voltage of 1000 Vpp. The voltage was measured using an oscilloscope (Hewlett Packard 54603B 60MHz), with a 10× probe (Kenwood PC-54, 600Vpp). An inverted microscope (Nikon Eclipse TE2000- U, Nikon Corporation, Tokyo, Japan) and an Andor Neo CMOS camera (Andor Technology, Belfast, Northern Ireland) were used to acquire the images and videos of the experiments. The images captured from the camera were recorded into a computer harddrive using NIS Element software (NIS Element Advanced Research v4.51, Nikon).

The beads used in the experiments are polystyrene beads, which usually have native sulfate groups on their surface. Therefore they are weakly negatively charged in common aqueous media. Polystyrene beads can be grafted with different kinds of charged groups at higher concentration than the native sulfate charge groups, giving them higher negative charge (as with carboxylate-modified or sulfate-modified beads) or positive charge (as with amine-modified beads). The beads were provided by commercial suppliers (Duke Scientific, Palo Alto, CA, USA or Invitrogen Molecular Probes, Eugene, Oregon, USA), suspended at 1 – 2% solid in DI water, with optionally added surfactant (for example 0.1% Tween<sup>®</sup> 20 or SDS) to ensure colloidal stability and 2 mM sodium azide as biocide.

In experiments, the beads were suspended in DI water with added chemicals for specific purposes. In electrokinetic DLD experiments, *KCl* was used to adjust conductivity and Polyvinylpyrrolidone (PVP), a water-soluble polymer, was optionally added to suppress electroosmotic flow.

# Chapter 5

## SUMMARY OF MANUSCRIPTS

### 5.1 Electrokinetic Deterministic Lateral Displacement

Beech *et al.* [34] showed the first use of low frequency AC voltage to enhance Deterministic Lateral Displacement (DLD), where dielectrophoresis helps adjust the critical diameter of the device, and hence, makes it possible to sort by dielectric properties. In this manuscript, the idea was developed further by considering both AC and DC and probing different parameters. It has been shown that due to difference in flow profile, a DC electrokinetic DLD device has a different critical diameter than a conventional pressure driven DLD, suggesting a possibility of tuning the critical diameter with a DC voltage. Experiments were also performed with particles of different surface charge densities and it was proven that surface charge can be an additional sorting parameter when AC voltage was applied on a DLD device, a property which can be exploited to sort cells of difference surface charge density or polarizability. Another conclusion was that the displacement of particles in an AC-enhanced DLD device was dependent on not only the strength of the field but also its frequency; both parameters can be used to tune the critical

diameter of the device. In future work, a further study on the interplay between AC electroosmosis and dielectrophoresis will promise not only an application to DLD but also to other techniques of microfluidics.

## **5.2 Dielectrophoretic effect on red blood cells in deterministic lateral displacement**

It has been proven previously that by controlling the depth of a DLD device, the orientation of red blood cells and thus their effective size can be changed. This effect was exploited to separate RBC from from trypanosome [18, 19], a critical step in diagnosis of the fatal disease *sleeping sickness*. It is then tempting to explore another method which can alter the orientation of red blood cells but is not limited to fabricating DLD devices with the specific depth. In this manuscript, it was demonstrated that by applying a low frequency AC voltage (100 Hz) of a nominal value of around  $177 V_{\text{RMS}}/\text{cm}$ , the orientation of red blood cells in deterministic lateral displacement (DLD) devices could be altered. Experiments showed that, due to this orientation change, the effective size of RBC can be increased by a factor of around 1.5, from below  $3.47 \mu\text{m}$  to  $4.44 \mu\text{m}$ . This can be useful in sorting non-spherical bio-particles, like RBC and trypanosome, benefiting the high throughput afforded by deep devices.

## **5.3 Sorting bacterial by chain length**

Many bacteria are pathogens causing serious diseases in humans. *S. pneumoniae* is a major cause of pneumonia which leads to more than one million deaths worldwide annually, and thus, is the subject of many humoral immunity studies. *S. pneumoniae* exist in their colony as either single bacteria or chains of many

bacteria with varying length. It is believed that longer chains can adhere more to epithelial cells in the lung while shorter chains and singles are better able to evade the immune system [35, 36]. Therefore, there is an interest in sorting these different morphologies for future detailed studies.

In this work, different hydrodynamic behavior of long and short chains of *S. pneumoniae* in a DLD device were exploited to fractionate them. With a device having the critical diameter approximately the size of a single coccus, single cocci were enriched in some outlets of the device and long chains were collected in the other ones. A high throughput device capable of sorting roughly a million of particles per minute was also designed, fabricated, and tested with polystyrene beads. In future work, the high throughput device will be used to sort *S. pneumoniae*.

# Chapter 6

## CONCLUSIONS AND OUTLOOK

In conclusion, the work presented in this thesis concerns about making use, improving, and adding functionalities to Deterministic Lateral Displacement, a high resolution, continuous, label-free particle sorting microfluidic technique. There are four main contributions of this work. First, it has been shown and explained how combining DC electrokinetics with DLD can help change the critical diameter of the device and thus suggests a tuning capability. Second, it was demonstrated that AC electrokinetics can add surface charge density as a new sorting parameter into DLD. Along the same line, AC electrokinetic DLD was revealed to be frequency-dependent, making frequency another parameter to tune a DLD device. Third, AC electrokinetic DLD was shown to be capable of changing the orientation of red blood cells in a DLD device, a property which can be exploited to sort red blood cells from, for example trypanosomes, as has been shown in earlier work by Holm *et al.* [18, 19]. Last but not least, it has been shown that DLD devices could be useful for microbiologists in helping them sort different chain lengths of *Streptococcus pneumoniae*, the main causes of pneumoniae, a serious disease in many developing countries of the world.

The above findings suggest several straight forward to-do tasks for future research. Firstly, as the high throughput DLD device has been characterized with

polystyrene beads and shown good separation and collection, the next step will be using the device for its targeted purpose, which is sorting different chain lengths of *S. pneumoniae*, aiming at a quantity relevant for RNA analysis. Secondly, further analysis and simulation should be carried out to understand more deeply about the underlying mechanisms of frequency-dependent AC electrokinetic DLD. This may bring about novel knowledge which will benefit not only DLD but also other applications of microfluidics, including sorting of other types of biological particles.

# Chapter 7

## POPULAR SCIENCE SUMMARY

Most of the visible things around us are solid: the chair you are sitting on, the building you are in, vehicles, constructions, trees, lab equipments, etc. This does not mean fluids - liquids and gases - are useless. In fact they are vital for humans life, like the fresh air you breath in and the water you drink, or simply just some coffee to keep you awake in the morning. The fact that there are few tools making use of fluids can be attributed to their high deformability. Fluids change their shape easily under an applied force, thus making it difficult to control or manipulate. Nevertheless, there are areas of science and technology where fluids are indispensable. Microfluidics is one such field.

Microfluidics refers to the study of liquids and gases at the micrometric scale – the scale of things that are smaller than the resolution limit of a human’s eyes, the world of tiny bio-particles like bacteria, parasites or red blood cells. There are several good reasons for studying such a difficult field. Firstly, in order to deal with cells and pathogens, we need to shrink our tools and devices down to their size! Secondly, making tiny devices also means that we need only a tiny amount of, say blood sample from patients, making diagnosis more economical and less painful. Last but not least, we might integrate those tiny tools and devices into a small chip, a lab-on-a-chip, and distribute them to the patients’ home where they

can do the diagnosis themselves, which is really the future of medical diagnostics.

In the theme of microfluidics, this thesis focuses on separating apart different kinds of cells by their physical properties, with the goal of making biomedical tools that are simpler, cheaper and more accesible to everyday's life. The three properties of interest in this work are size, shape, and electrical properties of the cells need to be sorted. Thanks to the disposability of the material, the simplicity of the mechanism (no complicated chemical needed), there are positive prospects of making the devices available to each person's home for them to perform the diagnosis by themselves or to distant regions of the world to help local people conduct useful medical tests which are inaccessible to them previously. The work in this thesis is a small step in the journey to that future.

# Appendix: Source code of a typical T-cell

T-cell stands for Template cell, a feature in L-Edit which allows users to draw parametric, adjustable geometric shapes, making it easy to design a device using a hierarchical approach. Below is the source code for the T-cell *Generate array*, which combines straight ends and periods into a DLD array, described in Section 4.2.

```
1 module Generate_Array_code {
2     #include <stdlib.h>
3     #include <math.h>
4     #include <string.h>
5     #include <stdio.h>
6     #include "ldata.h"
7     /* Begin -- Remove this block if you are not using L-Comp. */
8     #include "lcomp.h"
9     /* End */
10    /* TODO: Put local functions here. */
11    void Generate_Array_main(void) {
12        /* Begin DO NOT EDIT SECTION generated by L-Edit */
13        LCell    cellCurrent = (LCell)LMacro_GetNewTCell();
14        double   p = LCell_GetParameterAsDouble(cellCurrent, "p");
15        double   g = LCell_GetParameterAsDouble(cellCurrent, "g");
16        int      N = LCell_GetParameterAsInt (cellCurrent, "N");
17        int      S = LCell_GetParameterAsInt (cellCurrent, "S");
18        int      M = LCell_GetParameterAsInt (cellCurrent, "M");
```

```

19     int    A = LCell_GetParameterAsInt(cellCurrent, "A");
20     /* End DO NOT EDIT SECTION generated by L-Edit */
21     /* Begin -- Remove this block if you are not using L-Comp. */
22     LC_InitializeState();
23     LC_CurrentCell = cellCurrent;
24     /* End */
25     // Local variables
26     double x, y;
27     double n = (double) N;
28     int i;
29     // Scale to interal unit (1/1000 um)
30     double P, G;
31     P      = 1000*p;
32     G      = 1000*g;
33     // Parameters for the straight ends
34     const char* params[11];
35     params[0] = "p";
36     params[1] = LFormat("%f", p);
37     params[2] = "g";
38     params[3] = LFormat("%f", g);
39     params[4] = "N";
40     params[5] = LFormat("%d", M);
41     params[6] = "S";
42     params[7] = LFormat("%d", S);
43     params[8] = "E";
44     params[9] = LFormat("%d", 0); //not the last yet
45     params[10] = NULL;
46     LC_Generate ("Generate_Straight_End", "SE", params);
47     x = - P - G*sqrt(1/n) + (P+G)/n;
48     y = - N * (P+G);
49     LC_SetXYPlacementPosition (x, y);
50     // Parameter for the periods
51     params[5] = LFormat("%d", N);
52     for (int i = 1; i <= A; i++){
53         if (i == A) params[9] = LFormat("%d", 1);

```

```

54         // if it were the last array
55         LC_Generate ("Generate_Period", "P", params);
56         y = y - N * (P+G);
57         LC_SetXYPlacementPosition (x, y);
58     }
59     x = x + P + G*sqrt(1/n) - (P+G)/n;
60     y = y + (N-M) * (P+G);
61     LC_SetXYPlacementPosition (x, y);
62     params[5] = LFormat("%d", M);
63     LC_Generate ("Generate_Straight_End", "SE", params);
64 }
65 }
66 Generate_Array_main();

```

# Bibliography

- [1] E. Bassous, H. H. Taub, and L. Kuhn. Ink jet printing nozzle arrays etched in silicon. *Applied Physics Letters*, 31(2):135–137, 1977.
- [2] Stephen C. Terry, John H. Jerman, and James B. Angell. A gas chromatographic air analyzer fabricated on a silicon wafer. *IEEE Transactions on Electron Devices*, 26(12):1880–1886, 1979.
- [3] P. Gravesen, J. Branebjerg, and O. S. Jensen. Microfluidics-a review. *Journal of Micromechanics and Microengineering*, 3(4):168, 1993.
- [4] Younan Xia and George M. Whitesides. Soft lithography. *Annual review of materials science*, 28(1):153–184, 1998.
- [5] G. M. Whitesides. The origins and the future of microfluidics. *Nature*, 442(7101):368–73, 2006.
- [6] E. K. Sackmann, A. L. Fulton, and D. J. Beebe. The present and future role of microfluidics in biomedical research. *Nature*, 507(7491):181–9, 2014.
- [7] D. R. Gossett, W. M. Weaver, A. J. Mach, S. C. Hur, H. T. Tse, W. Lee, H. Amini, and D. Di Carlo. Label-free cell separation and sorting in microfluidic systems. *Anal Bioanal Chem*, 397(8):3249–67, 2010.
- [8] Jason Beech. *Microfluidics Separation and Analysis of Biological Particles*. PhD Thesis, Lund University, 2011.
- [9] G. K. Batchelor. *An Introduction to Fluid Dynamics*. Cambridge University Press, 2000.
- [10] L. R. Huang, E. C. Cox, R. H. Austin, and J. C. Sturm. Continuous particle separation through deterministic lateral displacement. *Science*, 304(5673):987–90, 2004.
- [11] D. W. Inglis, J. A. Davis, R. H. Austin, and J. C. Sturm. Critical particle size for fractionation by deterministic lateral displacement. *Lab Chip*, 6(5):655–8, 2006.
- [12] John Alan Davis. *Microfluidic separation of blood components through deterministic lateral displacement*. PhD thesis, Princeton University, 2008.

- [13] J. A. Davis, D. W. Inglis, K. J. Morton, D. A. Lawrence, L. R. Huang, S. Y. Chou, J. C. Sturm, and R. H. Austin. Deterministic hydrodynamics: taking blood apart. *Proc Natl Acad Sci U S A*, 103(40):14779–84, 2006.
- [14] Siyang Zheng, Raylene Yung, Yu-Chong Tai, and Harvey Kasdan. Deterministic lateral displacement mems device for continuous blood cell separation. In *Micro Electro Mechanical Systems, 2005. MEMS 2005. 18th IEEE International Conference on*, pages 851–854. IEEE, 2005.
- [15] Nan Li, Daniel T. Kamei, and Chih-Ming Ho. On-chip continuous blood cell subtype separation by deterministic lateral displacement. In *Nano/Micro Engineered and Molecular Systems, 2007. NEMS'07. 2nd IEEE International Conference on*, pages 932–936. IEEE, 2007.
- [16] K. Loutharback, J. D'Silva, L. Liu, A. Wu, R. H. Austin, and J. C. Sturm. Deterministic separation of cancer cells from blood at 10 ml/min. *AIP Adv*, 2(4):42107, 2012.
- [17] Z. Liu, F. Huang, J. Du, W. Shu, H. Feng, X. Xu, and Y. Chen. Rapid isolation of cancer cells using microfluidic deterministic lateral displacement structure. *Biomicrofluidics*, 7(1):11801, 2013.
- [18] S. H. Holm, J. P. Beech, M. P. Barrett, and J. O. Tegenfeldt. Separation of parasites from human blood using deterministic lateral displacement. *Lab Chip*, 11(7):1326–32, 2011.
- [19] S. H. Holm, J. P. Beech, M. P. Barrett, and J. O. Tegenfeldt. Simplifying microfluidic separation devices towards field-detection of blood parasites. *Anal. Methods*, 8(16):3291–3300, 2016.
- [20] J. P. Beech, S. H. Holm, K. Adolfsson, and J. O. Tegenfeldt. Sorting cells by size, shape and deformability. *Lab Chip*, 12(6):1048–51, 2012.
- [21] E. Henry, S. H. Holm, Z. Zhang, J. P. Beech, J. O. Tegenfeldt, D. A. Fedosov, and G. Gompper. Sorting cells by their dynamical properties. *Sci Rep*, 6:34375, 2016.
- [22] S. Chang and Y. H. Cho. A continuous size-dependent particle separator using a negative dielectrophoretic virtual pillar array. *Lab Chip*, 8(11):1930–6, 2008.
- [23] J. P. Beech, P. Jonsson, and J. O. Tegenfeldt. Tipping the balance of deterministic lateral displacement devices using dielectrophoresis. *Lab Chip*, 9(18):2698–706, 2009.
- [24] H. Morgan and N. G. Green. *AC Electrokinetics: Colloids and Nanoparticles*. Research Studies Press, 2003.
- [25] F. F. Reuss. Charge-induced flow. In *Proceedings of the Imperial Society of Naturalists of Moscow*, volume 3, pages 327–344, 1809.

- [26] J. O. M. Bockris, A. K. N. Reddy, and M. E. Gamboa-Aldeco. *Modern Electrochemistry 2A: Fundamentals of Electrode Processes*. Springer US, 2007.
- [27] Jean-Louis Viovy. Electrophoresis of dna and other polyelectrolytes: Physical mechanisms. *Rev. Mod. Phys.*, 72(3):813–872, 2000.
- [28] David Erickson. Electroosmotic flow (dc). In Dongqing Li, editor, *Encyclopedia of Microfluidics and Nanofluidics*, pages 560–567. Springer US, Boston, MA, 2008.
- [29] P. H. Paul, M. G. Garguilo, and D. J. Rakestraw. Imaging of pressure- and electrokinetically driven flows through open capillaries. *Anal. Chem.*, 70(13):2459–2467, 1998.
- [30] Miquel Sureda, Andrew Miller, and Francisco J. Diez. In situ particle zeta potential evaluation in electroosmotic flows from time-resolved micropiv measurements. *Electrophoresis*, 33(17):2759–2768, 2012.
- [31] E. B. Cummings, S. K. Griffiths, R. H. Nilson, and P. H. Paul. Conditions for similitude between the fluid velocity and electric field in electroosmotic flow. *Anal. Chem.*, 72(11):2526–2532, 2000.
- [32] Sandip Ghosal. Fluid mechanics of electroosmotic flow and its effect on band broadening in capillary electrophoresis. *Electrophoresis*, 25(2):214–228, 2004.
- [33] David W. Inglis. Efficient microfluidic particle separation arrays. *Applied Physics Letters*, 94(1):013510, 2009.
- [34] J. P. Beech and J. O. Tegenfeldt. Tuneable separation in elastomeric microfluidics devices. *Lab Chip*, 8(5):657–9, 2008.
- [35] J. L. Rodriguez, A. B. Dalia, and J. N. Weiser. Increased chain length promotes pneumococcal adherence and colonization. *Infect Immun*, 80(10):3454–9, 2012.
- [36] A. B. Dalia and J. N. Weiser. Minimization of bacterial size allows for complement evasion and is overcome by the agglutinating effect of antibody. *Cell Host Microbe*, 10(5):486–96, 2011.

# Manuscripts

Cite this: DOI: 10.1039/xxxxxxxxxx

## Electrokinetic Deterministic Lateral Displacement<sup>†</sup>

 Bao D. Ho,<sup>a</sup> Carlos Honrado,<sup>b</sup> Jason P. Beech,<sup>a</sup> Daniel Spencer,<sup>b</sup> Hywel Morgan,<sup>b</sup> and Jonas O. Tegenfeldt,<sup>\*a</sup>

 Received Date  
Accepted Date

DOI: 10.1039/xxxxxxxxxx

www.rsc.org/journalname

We report the use of surface charge as a new parameter for sorting in an AC Electrokinetic DLD device. Also, it was discovered that the displacement of particles in the AC Electrokinetic DLD was frequency-dependent which, as being confirmed by numerical simulation, is due to the interplay between Dielectrophoresis and Electroosmotic flow. The difference in critical diameter when using a pressure gradient versus a DC voltage to transport particles was also demonstrated and explained

### 1 Introduction

The separation, sorting, and enrichment of cells and bio-particles are important to many biomedical applications, especially diagnostics, therapeutics, and cell biology. Conventional cell sorting methods, including continuous flow cytometry, fluorescence-activated cell sorting (FACS), and magnetic-activated cell sorting (MACS)<sup>1</sup>, have been around for several decades and become familiar to biomedical researchers and technicians. However, those methods have several limitations: they require user specialization and training; the initial costs, operating costs, and reagent costs are high; and antibodies and fluorophores labeling may alter the functions of cells. For this reason, alternative cell sorting methods which are simple, low cost, and reagent-free are highly attractive. Instead of employing chemical labels or tags to identify cells of interest, label-free cell sorting exploits intrinsic physical properties to fractionate cells and it covers a wide range of different techniques targeting different physical properties of cells, including but not limited to size, shape, deformability, compressibility, density, dielectric properties, surface charge, et cetera.

In 2004, Huang *et al.* Princeton University proposed a novel label-free method for sorting particles based on size<sup>2</sup>. Their paper, published in *Science*, now has been cited for more than a thousand times. After more than ten years since its inception, *Deterministic Lateral Displacement* (DLD), has been used to sort WBC from RBC and plasma<sup>3, 4, 5</sup>, separate circulating moving cells from blood<sup>6, 7</sup> or separate trypanosome from blood<sup>8, 9</sup>.

Although originally being a size-based method, DLD has also been enhanced to sort particles based on other properties, for

example shape<sup>8, 9, 10</sup>, deformability<sup>10, 11</sup>, and electrical properties<sup>12, 13</sup>.

Electrokinetics has already been used in DLD to transport media and particles<sup>2, 13</sup>. Huang *et al.* used 0.1% POP-6 to suppress electroosmosis. In the latter, the authors allow both electroosmotic flow and electrophoresis of particles, but made a point that electroosmotic flow is much stronger than the other effect. One significant limitation of DC electricity, however, is the redox electrochemical reactions at the electrode, which may cause convective flow or generate bubbles. For this reason, AC electricity is a good alternative. Chang and Cho<sup>14</sup> also combined DLD and electricity but with AC and their device did not have any pillars at all. Instead, they use virtual pillars, which were gold electrode spots in a microfluidic channel to displace particles using dielectrophoretic force instead of steric force as in normal DLD, proving that *dielectrophoresis* (DEP) can be useful when combined with the DLD principle. Beech *et al.* had the same idea of combining DEP and DLD in their publication in 2009<sup>12</sup>, but in contrast to Chang and Cho, they employed real pillars made of PDMS as in conventional DLD and instead of electrode spots in the channel, platinum electrode rods were embedded in the inlet and outlet reservoirs, making fabrication simpler. It was demonstrated that by tuning the magnitude of the applied AC voltage, polystyrene beads of 3  $\mu\text{m}$  and 5  $\mu\text{m}$  could be separated, although they were inseparable in an otherwise conventional size-based DLD, demonstrating how DEP can enhance a conventional DLD device.

In this paper, we will take the idea of combining electrokinetics and DLD further. First, we perform the experiments of DC driven DLD but use Polyvinylpyrrolidone (PVP) to suppress electroosmotic flow and explain the mechanism. The relation between electroosmotic flow and electrophoresis of particles is also analyzed. Secondly, the dependence of dielectrophoretic-enhanced DLD on applied frequency is investigated and explained. Finally, we explore the possibility of using surface charge as a marker to

<sup>a</sup> Division of Solid State Physics and NanoLund, Lund University, Professorgatan 1, 22363 Lund, Sweden. E-mail: jonas.tegenfeldt@ftf.lth.se

<sup>b</sup> Faculty of Physical Sciences and Engineering, Institute for Life Sciences, University of Southampton SO17 1BJ, UK

<sup>†</sup> Electronic Supplementary Information (ESI) available: [details of any supplementary information available should be included here]. See DOI: 10.1039/b000000x/

separate particles.

## 2 Theory

### 2.1 DLD

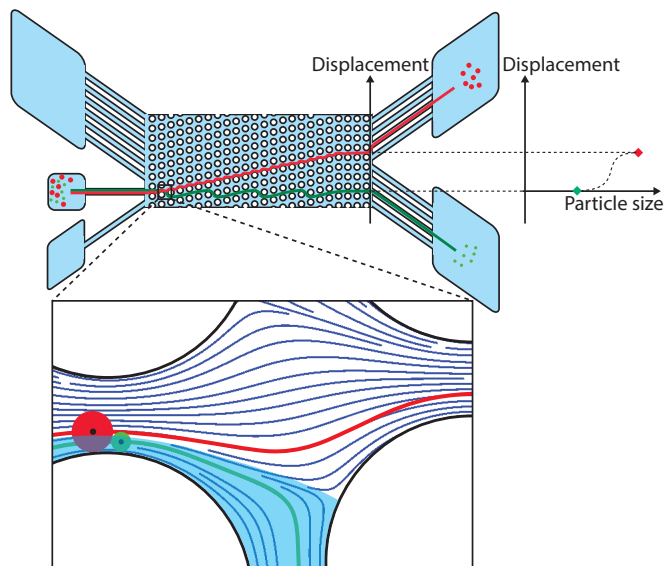


**Fig. 1** The principle of DLD. The schematic of the device is shown on the top, capable of sorting big (red) and small (green) particle in two populations. The inset at the bottom illustrates the mechanism. The solid blue area represents the liquid flow between the two pillars at the bottom. The particles which are smaller than the critical size will move with this liquid.

The mechanism of particles being sorted by size in DLD has been clearly explained by Huang *et. al.*<sup>2</sup>. We summarize the principle of DLD in Figure 1. We call a line of pillars perpendicular to the flow direction a *row*. Each row along the flow direction is shifted a small distance laterally with respect to the previous row. This asymmetric arrangement causes the flow to bifurcate when it encounters a pillar, as can be seen at the bottom of Figure 1: a small stream of the flow, painted in light blue, goes around under the pillar while the rest keeps going straight above the pillar. If the centre of the particle resides within the small stream (the green particle), it will also go around under the pillar while the bigger one (the red particle) whose centre does not fit into the blue stream will travel above the pillar. This separation is accumulated along the device causing different trajectories of the green and the red particles: one going zig-zag with zero net displacement in the perpendicular direction to the flow and the other being pushed continuously and ending up being *deterministically laterally displaced* at the end of the array.

The *critical diameter*, which is the threshold diameter at which particles switch from zig-zagging to displacement, can be estimated by the empirical formula proposed by John Davis<sup>15</sup>:

$$D_C = 1.4GN^{-0.48} \quad (1)$$

Where  $D_C$  is the critical diameter,  $G$  is the gap between two posts in a row, and  $N$  is the period of the array (the pillars in row  $N + 1$  have the same lateral positions as the pillars in row 1).

### 2.2 Electroosmotic flow and Electrophoresis

*Electroosmotic flow* refers to the transport of a solution of dissolved ions using an electric field and *electrophoresis* is defined as the transport of a charged particle using an electric field. Both phenomena can be explained by the theory of *electrical double layer*<sup>16</sup>. In fact, in the limit of a thin double layer, which is the case for channel walls in microfluidic devices and particles in the micrometer scale and above, the two phenomena have the same mechanism: the electric field exerts electrostatic force on the excessive charges in the diffuse layer of the double layer, and in turn these charges transfer the momentum they get via viscous drag to the element that is mobile in relation to the field (the liquid in electroosmosis and the particles in electrophoresis). This results in the movement of the liquid relative to the wall (electroosmotic flow) or the movement of charge particles relative to the liquid (electrophoresis).

The electroosmotic velocity or the electrophoretic mobility is quantified by the Helmholtz– Smoluchowski equation<sup>17,18</sup>:

$$u_{EOF} = -\frac{\epsilon\zeta_W}{\eta}E \quad (2)$$

$$u_{EP} = \frac{\epsilon\zeta_P}{\eta}E \quad (3)$$

Where  $\epsilon$  is the permittivity of the medium,  $\zeta$  is the zeta-potential at the shear plane (the subscript W and P mean wall and particle, respectively),  $\eta$  is the viscosity of the medium and  $E$  is the applied field.

It is convenient to define the *electroosmotic mobility* (and *electrophoretic mobility*) which is the ratio between the electroosmotic velocity (and the electrophoretic velocity) to the external electric field:

$$\mu_{EOF} = \frac{u_{EOF}}{E} = -\frac{\epsilon\zeta_W}{\eta}$$

$$\mu_{EP} = \frac{u_{EP}}{E} = \frac{\epsilon\zeta_P}{\eta}$$

### 2.3 DEP

The DEP force,  $\mathbf{F}_{DEP}$ , on a spherical particle of radius  $a$  in a non-uniform electric field  $\mathbf{E}$  is calculated as:

$$\mathbf{F}_{DEP} = \pi\epsilon_m a^3 Re \left( \frac{\tilde{\epsilon}_p - \tilde{\epsilon}_m}{\tilde{\epsilon}_p + 2\tilde{\epsilon}_m} \right) \nabla |\mathbf{E}|^2 \quad (4)$$

where  $\tilde{\epsilon}_m$ ,  $\tilde{\epsilon}_p$  are the complex permittivities of the particle and the suspending medium, defined as:  $\tilde{\epsilon} = \epsilon - i\sigma/\omega$ . Here  $\epsilon$  is the permittivity of the particle or the medium,  $\sigma$  is the conductivity of the particle or the medium and  $\omega$  is the angular frequency of the electric field. One should note that Eq. 4 applies well only when the magnitude of the electric field does not vary significantly across the dimensions of the particle<sup>19</sup>.

## 3 Experimental

### 3.1 Devices, materials, and methods

**Devices** were fabricated in polydimethylsiloxane (PDMS) using soft lithography<sup>20</sup>. A layer of 10  $\mu\text{m}$  SU8 (MicroChem, New-

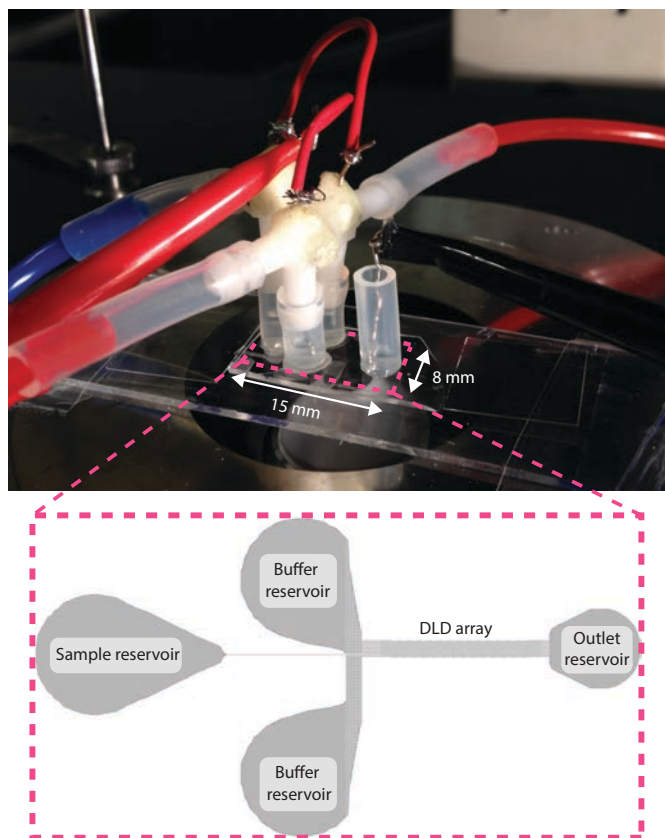


**Fig. 2** The experimental setup. (Top) Device connected to pressurized tubing and to platinum wires for application of voltage. (Bottom) Outline of device with reservoirs and DLD arrays.

ton, MA, USA) was spin coated onto a 3-inch silicon wafer and patterned using UV light in a contact mask aligner (Karl Suss, Munich, Germany). The SU8 master was then coated with an anti-sticking layer of tridecafluoro-(1,1,2,2)-tetrahydrooctyl-trichlorosilane (F13-TCS) (Sigma Aldrich, Saint Louis, MO, USA) to promote demolding of PDMS from the master later on. To make the PDMS device, PDMS monomer and curing agent (Sylgard 184, Dow Corning, Midland, MI, USA) in liquid state were mixed (10 : 1), degassed by a vacuum pump, poured onto the master and baked for 1 hour at 80°C. The PDMS slab was then peeled off from the mold and trimmed; 1 mm access holes were punched in the PDMS slab. The PDMS slab was then oxidized with oxygen plasma (Plasma Preen II-862, Plasmatic Systems, Inc, North Brunswick, NJ, USA) and bonded to a PDMS-coated microscope slide. Finally, silicone tubes were glued to the device at the access holes using silicone adhesive (Elastosil AO7, RTV-1 silicone rubber, Wacker Silicones, Munich, Germany).

**Equipment and setups.** Pressure-driven flow was created by an over pressure: a MFCS – 4C pressure controller (Fluigent, Paris, France) provided a pressure higher than the atmospheric pressure to all the inlet reservoirs as shown in Figure 2 and the outlet reservoirs were let open to the air. The device in Figure 2 had only one outlet to simplify analysis; when actual separation is required, a device with more than one outlet reservoir is

needed. Typical pressures used were between 10 mBar and 100 mBar, depending on the length of the device and the desired flow rate.

DC or AC fields were generated with a function generator (15 MHz function/arbitrary waveform generator, model 33120A, Hewlett Packard, Palo Alto, CA, USA) and amplified 100 times (Bipolar operational power supply/amplifier, model BOP 1000M, Kepco, Flushing, NY, USA) to give a maximum voltage of 1000 Vpp. The voltage was measured using an oscilloscope (Hewlett Packard 54603B 60MHz), with a 10× probe (Kenwood PC-54, 600Vpp). We use an inverted microscope (Nikon Eclipse TE2000-U, Nikon Corporation, Tokyo, Japan) and an Andor Neo CMOS camera (Andor Technology, Belfast, Northern Ireland) to acquire the images and videos of devices and particles. NIS Element software (NIS Element Advanced Research v4.51, Nikon) was used to store the images captured from the camera into a computer harddrive.

To apply both pressure and voltage at the inlet reservoirs, holes were drilled through T-connectors and platinum electrodes were embedded into the medium in the inlet wells through these holes, as shown in Figure 2. At outlet reservoirs, electrodes were also embedded.

**Media and beads.** The media used was a solution of KCl in de-ionized water, with polyvinylpyrrolidone (PVP) to avoid electroosmosis (optional, 1-2.5% (w/v)). The chemicals were bought from Sigma Aldrich (Sigma Aldrich, Saint Louis, MO, USA). Polystyrene microspheres with different fluorescent colors and different surface charge coating were used (Thermo Scientific).

### 3.2 Simulation

To correlate and explain the results, numerical simulations were performed using a finite element analysis software, COMSOL Multiphysics 5.0 (COMSOL, Inc., Burlington, MA, USA). Most of the simulations were done in 2D, as full field 3D simulation often requires much larger amount of mesh elements and thus, takes much more time to compute. Nevertheless, since most of the structures in the devices are 2.5D (3D extrusion of a 2D drawing), 2D simulation yielded sufficiently accurate results in many cases. An overview of the simulations is given below and more details can be found in Table 1 of the ESI.

*i. Laminar flow* is used for calculating the velocity profile of the fluid in the devices. Since the Reynold number of microfluidic devices is well below unity, inertial component can be neglected. Also, since the fluid velocity is well below the speed of sound, the flow is assumed incompressible. The wall boundary condition can be non-slip (pressure driven flow) or slip boundary condition (electroosmotic flow).

*ii. Wall distance* helps calculate the distance from the centre of mass of a particle to a wall to apply a wall (steric) force.

*iii. Electric current* solves for electric field in the device, which will be used to calculate electroosmotic flow and dielectrophoresis force.

*vi. Particle tracing for fluid flow* simulates dynamics of the particles in a DLD device under combined action of pressure driven

flow, electroosmotic flow, electrophoresis and dielectrophoresis.

To optimize computation time, simulations were done at different scales:

*i. Device:* The whole device was drawn in COMSOL and laminar flow and electric current were solved. The purpose of this was to find out the voltage and pressure drop across the whole array. This step could consume considerable amount of memory and computation time.

*ii. Array:* The voltage and pressure calculated in the previous step were used as the boundary condition for this step. Laminar flow and electric current physics were solved again, only at finer mesh to obtain more accurate solutions.

*iii. Single period:* In a single period in the middle of the array, wall distance and particle tracing for fluid flow physics were solved at even finer mesh. Solving the velocity and electric field in the whole device gives us realistic boundary conditions with which to solve in a smaller area at much higher resolution. The geometry simulated in step *i.*, *ii.*, *iii.* are illustrated in Figure 1 of the ESI.

### 3.3 Combine DLD with DC

Carboxylate-modified beads with diameter of  $2\ \mu\text{m}$  were suspended in  $25\ \text{mS/m}$  KCl,  $2.5\ \text{wt\%}$  PVP. The setup and the device have already been shown in Figure 2; the device has the period of 10, gap width of  $5\ \mu\text{m}$  and the critical diameter of  $2.3\ \mu\text{m}$ , using Equation 1. Either a pressure or a DC voltage were applied and trajectories of beads were observed and recorded. The applied pressure or voltage reported in this paper were defined as:  $P_{\text{applied}} = P_{\text{inlet}} - P_{\text{outlet}}$  and  $V_{\text{applied}} = V_{\text{inlet}} - V_{\text{outlet}}$ .

A combination of pressure driven flow and DC driven flow was also investigated. In this experiment, the same beads were used ( $2\ \mu\text{m}$  carboxylate-modified) but the medium was different ( $28\ \text{mS/m}$  KCl,  $1.0\ \text{wt\%}$  PVP, but this time PVP was not part of the running medium. It was flushed through the device in 10 minutes before the experiment were carried out). The device has the period of 10, gap width of  $8\ \mu\text{m}$  and the critical diameter of  $3.7\ \mu\text{m}$ , using Equation 1. The pressure was kept at  $5\ \text{mBar}$  and the voltage was scanned so that the DC driven flow balanced out the pressure driven flow, the condition at which the beads had no net velocity.

### 3.4 Sorting by surface charge

Surface charge can be a good marker to identify cells. For example, even with one cell type, surface charge can vary within one cell cycle<sup>21</sup>. Therefore, it is desirable to sort cells based on their surface charge. We investigated this possibility by employing DLD in combination with an AC field. With the same setup as shown in Figure 2, a DLD device having multiple critical diameters in series was used. It was designed by changing the number of rows in one period,  $N$ , after several periods, while keeping the gap width the same through out the array. The number of rows in one period is in the range:  $N_i = 30, 20, 15, 10, 6, 5, 4, 3, 2$ , corresponding to the critical diameter of:  $D_{Ci} = 1.5, 1.8, 2.1, 2.5, 3.2, 3.5, 3.9, 4.5, 5.4\ \mu\text{m}$ , respectively, where  $i$  runs from 1 to 8. The medium used was TBE  $0.5\times$ , SDS

$0.1\%$ , PVP  $2.0\ \text{wt\%}$ , the conductivity was estimated to be  $0.2\ \text{S/m}$ . Two kinds of beads were used, having similar sizes but different surface modification:  $2.1\ \mu\text{m}$  plain beads (with native sulfate groups on surface) (Duke Science, Palo Alto, CA, USA) and  $2.0\ \mu\text{m}$  carboxylate-modified beads (Invitrogen Molecular Probes, Eugene, Oregon, USA). Plain beads with native surface groups on surface has relatively low surface charge, just enough for stabilizing the beads in solution, whereas carboxylate-modified beads from Molecular Probes has the surface charge ranges between  $0.1$  and  $2.0$  milliequivalents/gram<sup>22</sup>. For a bead of  $2.0\ \mu\text{m}$  in diameter, this means a range of negative  $0.2 - 5 \times 10^9$  elementary charge. A pressure of  $60\ \text{mBar}$  and a  $100\ \text{Hz}$  AC voltage of up to  $1000\ V_{pp}$  was applied. Closed-up videos were taken near the outlet of the device and beads were counted to study the distribution of their lateral displacement at different applied voltage.

### 3.5 Frequency dependence of AC-enhanced DLD devices

When Beech and his colleagues explored using AC field to tune DLD devices<sup>12</sup>, their main focus was on the strength of the electric field, i.e. the root mean square or peak-to-peak value of the voltage, but not the frequency of the field because the DEP force in their experiments was mostly independent of the frequency due to the high conductivity of the medium. In fact, this independence is a universal property of DEP force for AC frequency up to around  $100\ \text{kHz}$ , which can be proved as follows.

The real part of the Clausius-Mossotti factor can be written in terms of permittivity and conductivity of particle and medium:

$$Re(f_{CM}) = \frac{\omega^2 (\epsilon_p - \epsilon_m) (\epsilon_p + 2\epsilon_m) + (\sigma_p - \sigma_m) (\sigma_p + 2\sigma_m)}{\omega^2 (\epsilon_p + 2\epsilon_m)^2 + (\sigma_p + 2\sigma_m)^2} \quad (5)$$

The permittivities of polystyrene and water are known:  $\epsilon_p = 2.55\epsilon_0$  and  $\epsilon_m = 78.5\epsilon_0$ . If the conductivity of the particle is assumed to have a nominal value of  $\sigma_p = 2\ \text{mS/m}$ , the order of magnitude of frequency at which the permittivities and the conductivities have approximately the same contribution to  $Re(f_{CM})$  is:

$$f_1 = \frac{\sigma_p}{2\pi\epsilon_m} = \frac{0.002}{2 \times 3.14 \times 78.5 \times 8.85 \times 10^{-12}} \approx 2 \times 10^6 (\text{Hz})$$

Below this frequency range, the conductive effect is dominant in  $Re(f_{CM})$  and Equation 5 can be estimated as:

$$Re(f_{CM}) \approx \frac{\sigma_p - \sigma_m}{\sigma_p + 2\sigma_m}$$

, which is independent of frequency.

However, when an AC field is applied, besides DEP there are also electroosmotic effect, as can be seen in Section 4.1. At low frequency (below  $1000\ \text{Hz}$ ), the particles would oscillate back and forth due to the variation of the field and the amplitude of this oscillation is frequency-dependent. Therefore, it is anticipated that the dynamics of the particles in an AC-enhanced DLD device may be influenced by the frequency of the applied voltage.

To investigate this matter, experiments were performed with

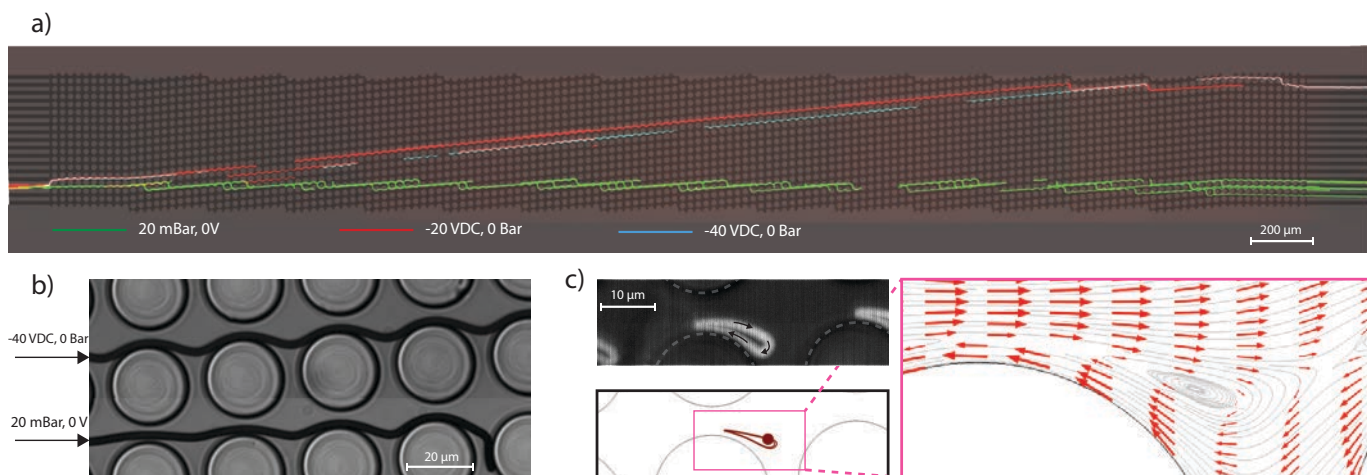


**Fig. 3** Combining DLD with DC voltage. (a)  $2\ \mu\text{m}$  carboxylate-modified beads went zigzag in a DLD array with a pressure driven flow and went displaced with a DC driven flow. (b) A close-up view of the trajectories in Figure (a). (c) When combining pressure driven flow and DC driven flow, in the case when the two flow had relatively equal strength, the beads went in an airfoil loop near the pillars. The phenomenon was confirmed by simulations.

carboxylate-modified beads ( $2\ \mu\text{m}$ ) suspended in  $22\ \text{mS/m}$   $\text{KCl}$ ,  $2.5\ \text{wt}\%$   $\text{PVP}$  medium. The setup has already been shown in Figure 2; the device has the period of 10, gap width of  $5\ \mu\text{m}$  and the critical diameter of  $2.3\ \mu\text{m}$ , using Equation 1. A pressure of 30 mBar was used to transport the particles and AC sinusoidal signals with frequency  $f = 20 - 5000\ \text{Hz}$ , voltage  $V = 75 - 300\ \text{V}_{\text{PP}}$  were applied. Videos were captured inside the array and at the outlet of the devices and the lateral position where particles appeared at the outlet at different voltage and frequency were noted.

A numerical simulation was set up to explain the mechanism. A pressure driven flow was simulated in the array with boundary conditions being the pressure between the two ends of the array. An AC voltage was also applied between the two ends of the array; the electric field calculated in the electric current physics was used to simulate the electroosmotic flow and the dielectrophoretic force on the particle. The particle trajectories at different frequencies was calculated and compared.

## 4 Results and discussion

### 4.1 Combine DLD with DC electricity

The trajectories of beads at different applied pressure and DC voltages were shown in Figure 3 a) and the close-up trajectories were shown in Figure 3 b). As shown in the figure, the beads go zig-zagging in the pressure-driven flow and displace in the DC-driven flow. This phenomenon is due to the difference in the flow profiles of the pressure-driven flow and the DC-driven flow. When a pressure is applied, the fluid is static at the wall (non-slipping boundary condition), thus, the flow has a parabolic profile in the gap between two pillars along flow direction. When a DC field is applied, the beads are guided by both electroosmotic flow and by particle electrophoresis. Both effects have the same plug-like characteristics: the flow profile is flat in the gap between two pillars along the flow direction. For a device having the gap width  $G$  and the period  $N = 10$ , calculation revealed that:  $D_{C/\text{parabolic}} = 0.4G$  and  $D_{C/\text{plug}} = 0.2G$ . For  $G = 5\ \mu\text{m}$ ,

$D_{C/\text{parabolic}} = 2\ \mu\text{m}$  and  $D_{C/\text{plug}} = 1\ \mu\text{m}$ . This explains why a particle  $2\ \mu\text{m}$  big traveled in zig-zagging mode in pressure driven flow but displaced in DC driven-flow.

The closed-up trajectories when pressure driven flow and DC driven flow were balanced were shown in Figure 3 c), together with simulation results of particle trajectories (below the experimental image) and the streamlines and vectors of fluid velocity on the right hand side. As shown in Figure 3 c), the particle was maneuvered in a loop close to the edge of a pillar. This can be explained by the combined action of a pressure-driven flow and an DC-driven electroosmotic flow, in opposite direction. Since parabolic flow is stronger in the middle while electroosmotic flow is stronger close to the walls, when they are in opposite direction, there would be vortices close to the walls and the particles would be trapped if they slip into such close loop flow streams.

### 4.2 Sorting by surface charge

As can be seen on Figure 4, when the applied voltage was ramped up, the lateral displacement was increased for both kinds of beads. However, the dependence of the displacement on the voltage was different for different kinds of beads. From the displacement values on the left vertical axis, the effective diameter of the particles can be estimated. Here we define the effective diameter as the diameter of a hard spherical particle that would follow an identical trajectory through the same DLD device but without an applied voltage. While the effective diameter of sulphate beads were changed from around  $2\ \mu\text{m}$  to  $2.5\ \mu\text{m}$  by an applied voltage of  $900\ \text{V}_{\text{PP}}$ , that of carboxylate-modified beads was from  $1.8\ \mu\text{m}$  to  $3.9\ \mu\text{m}$ , showing that surface charge clearly had an effect in the AC-enhanced DLD device. The explanation will follow in the next section.

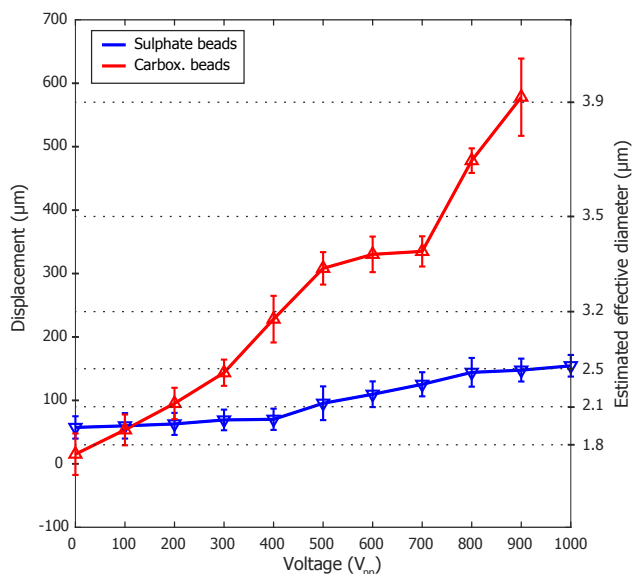


**Fig. 4** Displacement (left) and estimated effective diameter of beads (right), as a function of applied voltage. The beads were driven by a pressure of 60 mBar.

### 4.3 Frequency dependence of AC-enhanced DLD devices

As shown in Figure 5 a), as the frequency increased, the particle became more zig-zagging: first, at the dotted green position of the figure, the particle stayed closer to the pillars; second, at the dotted red position, the particle descended deeper into the valley in between the pillars. The exiting positions of the particles at the outlet of the device were plotted in Figure 5 b), as a function of frequency, at three different peak-to-peak voltage values. The graph shows a consistent trend with the the images in Figure 5 a): the displacement effect got weaker when the frequency increased and reduced to almost none at 5000 Hz.

The simulation results in Figure 6 show a consistent trend with experimental results that at higher frequency, the particle tends to go zig-zag, although in the model, the DEP was set to be the same for all three cases. It is possible that there has been an interplay between the DEP force and the oscillation due to electroosmosis of the particle. Although the mechanism is still obscure, it is clear from the figure that the trajectory at 100 Hz, due to high amplitude of oscillation, has been “pushed” out more into the middle of the flow and thus, has a greater tendency to be displaced.

## 5 Conclusions

We have demonstrated a combination of AC/DC electrokinetics and DLD. Firstly, we have shown that a DC electrokinetic DLD device has a different critical diameter than a conventional pressure driven DLD, suggesting a possibility of tuning the critical diameter with a DC voltage. Secondly, surface charge was proven to be an additional sorting parameter when AC voltage was applied on a DLD device, a property which can be exploited to sort cells of difference surface charge density or polarity. Last but not least, it was discovered that the displacement of particles in an AC-enhanced DLD device was dependent on not only the strength of the field but also its frequency; both parameters can be used

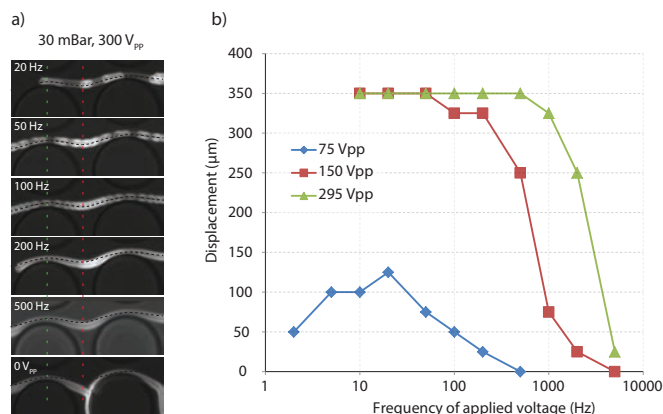


**Fig. 5** a) Influence of AC frequency on trajectories of a bead. The trajectory of the bead at 100 Hz (dotted black line) was added to all images as a reference. b) Displacement of the beads at the outlet of the device as a function of the AC frequency, at different voltage.

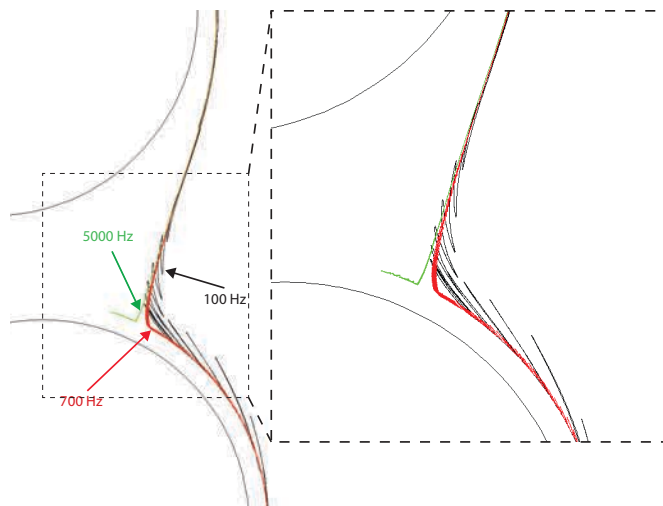


**Fig. 6** a) Influence of AC frequency on trajectories of a bead. The trajectory of the bead at 100 Hz (dotted black line) was added to all images as a reference. b) Displacement of the beads at the outlet of the device as a function of the AC frequency, at different voltage.

to tune the critical diameter of the device. In a future work, a further study on the interplay between AC electroosmosis and dielectrophoresis will promise not only an application to DLD but also to other techniques of microfluidics.

## References

- 1 D. R. Gossett, W. M. Weaver, A. J. Mach, S. C. Hur, H. T. Tse, W. Lee, H. Amini and D. Di Carlo, *Anal Bioanal Chem*, 2010, **397**, 3249–67.
- 2 L. R. Huang, E. C. Cox, R. H. Austin and J. C. Sturm, *Science*, 2004, **304**, 987–90.
- 3 J. A. Davis, D. W. Inglis, K. J. Morton, D. A. Lawrence, L. R. Huang, S. Y. Chou, J. C. Sturm and R. H. Austin, *Proc Natl Acad Sci U S A*, 2006, **103**, 14779–84.
- 4 S. Zheng, R. Yung, Y.-C. Tai and H. Kasdan, 18th IEEE International Conference on Micro Electro Mechanical Systems,

2005. *MEMS 2005.*, 30 J, pp. 851–854.
- 5 N. Li, D. T. Kamei and C. M. Ho, 2007 2nd IEEE International Conference on Nano/Micro Engineered and Molecular Systems, 16-1, pp. 932–936.
- 6 K. Louthback, J. D'Silva, L. Liu, A. Wu, R. H. Austin and J. C. Sturm, *AIP Adv*, 2012, **2**, 42107.
- 7 Z. Liu, F. Huang, J. Du, W. Shu, H. Feng, X. Xu and Y. Chen, *Biomicrofluidics*, 2013, **7**, 11801.
- 8 S. H. Holm, J. P. Beech, M. P. Barrett and J. O. Tegenfeldt, *Lab Chip*, 2011, **11**, 1326–32.
- 9 S. H. Holm, J. P. Beech, M. P. Barrett and J. O. Tegenfeldt, *Anal. Methods*, 2016, **8**, 3291–3300.
- 10 J. P. Beech, S. H. Holm, K. Adolfsson and J. O. Tegenfeldt, *Lab Chip*, 2012, **12**, 1048–51.
- 11 E. Henry, S. H. Holm, Z. Zhang, J. P. Beech, J. O. Tegenfeldt, D. A. Fedosov and G. Gompper, *Sci Rep*, 2016, **6**, 34375.
- 12 J. P. Beech, P. Jonsson and J. O. Tegenfeldt, *Lab Chip*, 2009, **9**, 2698–706.
- 13 S. Hanasoge, R. Devendra, F. J. Diez and G. Drazer, *Microfluidics and Nanofluidics*, 2014, **18**, 1195–1200.
- 14 S. Chang and Y. H. Cho, *Lab Chip*, 2008, **8**, 1930–6.
- 15 J. A. Davis, *PhD thesis*, Princeton University, 2008.
- 16 J. O. M. Bockris, A. K. N. Reddy and M. E. Gamboa-Aldeco, *Modern Electrochemistry 2A: Fundamentals of Electrodeics*, Springer US, 2007.
- 17 J.-L. Viovy, *Rev. Mod. Phys.*, 2000, **72**, 813–872.
- 18 D. Erickson, *Encyclopedia of Microfluidics and Nanofluidics*, Springer US, Boston, MA, 2008, pp. 560–567.
- 19 H. Morgan and N. G. Green, *AC Electrokinetics: Colloids and Nanoparticles*, Research Studies Press, 2003.
- 20 Y. Xia and G. M. Whitesides, *Annual review of materials science*, 1998, **28**, 153–184.
- 21 T. P. Brent and J. A. Forrester, *Nature*, 1967, **215**, 92–93.
- 22 M. Probes, *Working with FluoSpheres Fluorescent Microspheres*, 2004.

# Electronic supplement information

June 2, 2017

Physics	Differential equations/Boundary conditions	Meaning
Laminar flow	$0 = \nabla \cdot [-p\mathbf{I} + \mu(\nabla\mathbf{u} + (\nabla\mathbf{u})^T)] + \mathbf{F}$	Inertial term neglected (left hand side), surface forces and body forces adds up to zero (RHS).
	$\rho\nabla\cdot\mathbf{u} = 0$	Incompressible flow
	$\mathbf{u} = 0 _{walls}$	No-slip boundary condition
	$\mathbf{u} = \mu_{EO}\mathbf{E}_t _{walls}$	Electroosmotic flow boundary condition
	$p = p_0 _{inlet}, p = 0 _{outlet}$	Pressure at the inlet and outlet of the device
Wall distance	$ \nabla D  = 1$	The norm of the gradient of wall distance is unity
	$D = 0 _{wall}$	Wall distance is zero for the points on the wall
Electric current	$\nabla\cdot\mathbf{J} = 0$	Continuity equation of current
	$\mathbf{J} = \sigma\mathbf{E}$	Ohm's law in steady state
	$\mathbf{J} = (\sigma + j\omega\varepsilon_0\varepsilon_r)\mathbf{E}$	Ohm's law in frequency domain
	$\mathbf{J} = (\sigma + \varepsilon\varepsilon_r\frac{\partial}{\partial t})\mathbf{E}$	Ohm's law in transient state
	$\mathbf{E} = -\nabla V$	Definition of electric potential
	$V = V_0 _{inlet}, V = 0 _{outlet}$	Voltage at the inlet and outlet of the device
Particle tracing for fluid flow	$\frac{d}{dt}(m_p\mathbf{v}) = \mathbf{F}_t$	Newton's second law
	$\mathbf{F}_D = \frac{1}{\tau_p}m_p(\mathbf{u} - \mathbf{v})$ $\tau_p = \frac{\rho_p d_p^2}{18\mu}$	Drag force, Stokes form used for laminar flow Particle velocity response time for spherical particles in a laminar flow
	$\mathbf{F}_w = F_{w0} \times \text{step}(D - r_p) \times (-\mathbf{D}_{dir})$	Wall repulsive force
	$\mathbf{F}_{DEP} = 2\pi r_p^3 \varepsilon_m Re\{f_{CM}\} \nabla  \mathbf{E}_{rms} ^2$ $f_{CM} = \frac{\varepsilon_p^* - \varepsilon_m^*}{\varepsilon_p^* + 2\varepsilon_m^*}$ $\varepsilon^* = \varepsilon - j\frac{\sigma}{\omega}$	Dielectrophoresis force The Clausius-Mosotti factor Complex permittivity

Table 1: Modules used in numerical simulation using COMSOL

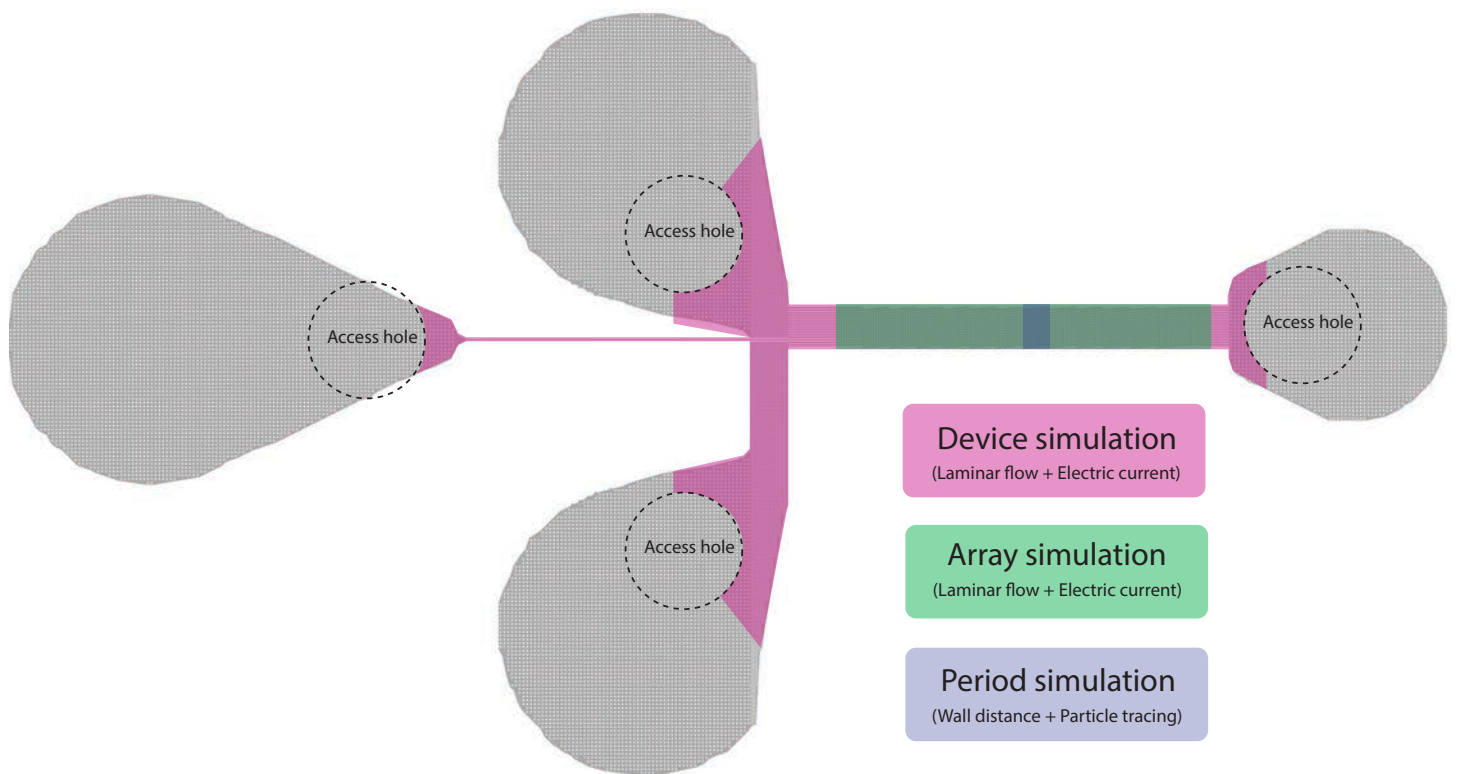


Figure 1: Simulation domains. To optimize computation time, simulations were done in bigger domains first, then the results were used as boundary conditions of simulations of smaller domains. Since a period is much smaller than an array or a device, simulations ran much faster there, allowing for using finer mesh for more accurate solution or repeat with different parameters.

# Dielectrophoretic effect on red blood cells in deterministic lateral displacement devices

Bao D. Ho,<sup>a</sup> Hasti Yavari,<sup>b</sup> Stefan H. Holm,<sup>a</sup> Si-Hoai-Trung Tran,<sup>a</sup> Jason P. Beech,<sup>a</sup> Jonas O. Tegenfeldt<sup>\*a</sup>

**Abstract:** We report a biological application of dielectrophoresis (DEP) in changing the orientation of red blood cells in deterministic lateral displacement (DLD) devices. DEP has been shown in other work to have the ability of changing the effective size of spherical polystyrene particles in a DLD device, offering the option of sorting by electrokinetic effect besides steric effect (size-based sorting). Our work demonstrates that DEP can also change the effective size of a particle, in this case red blood cell, by a more sophisticated way, which is by modifying its orientation in laminar flow. The experiments showed that by applying a low frequency AC voltage (100 Hz) of around 177 V<sub>RMS</sub>/cm in an isotonic buffer, the RBCs exhibit negative dielectrophoretic property and their effective size can be increased by a factor of around 1.5, from below 3.47 μm to 4.44 μm. Our work indicates that DEP-DLD device can find a wide range of applications in biological sorting, in particular for separation of RBCs from other kinds of cells and pathogens.

## 1. Introduction

Particle separation is important for various applications ranging from clinical pharmacology to diagnostic devices in the field of medicine and biology. One particular sample widely used in clinical studies is blood consisting of different cells such as white blood cells (WBCs) a.k.a leukocytes, red blood cells (RBCs) a.k.a erythrocyte and platelets. Under different physiological circumstances, distinct morphological changes are observed in RBCs affecting the cell's deformability. The extent of this deformation varies for different disease pathologies. For instance, cancerous blood cells are known to have a more deformable phenotype as opposed to healthy cells<sup>1</sup> whereas less deformable phenotype is observed in the case of Sickle-cell disease (SCD) and Malaria.<sup>2</sup> In malaria higher stiffness of the parasitized RBCs is exhibited for more advanced stages of the disease. In addition the physical and mechanical properties of a particle change with its size. Therefore valuable information about the state of health or the phase in cycle of an individual cell can be extracted by investigating the cells physical properties.

The techniques dominantly used for blood cell separation are fluorescence activated cell sorting (FACS) and magnetic-activated cell sorting (MACS) yielding high resolution results with the downside of being intrusive as sample labeling needs to be done. In recent years different microfluidic particle separation devices have been introduced as a cheaper, more flexible and less time consuming alternative technique. One particular advantage of these devices is the ability of working at nanometer or micrometer scale relative to the size of the particles being investigated.

Deterministic lateral displacement is a fundamental microfluidic separation technique introduced by Huang et al. in 2004, where particle separation based on size was reported with resolution as low as 10 nm.<sup>3</sup> The particle separation in this passive device is done based on internal forces of the particular geometry of the design. One positive characteristic of DLD is its good integration ability with other components. In 2008, Chang and Cho introduced a virtual DLD device with varying critical size.<sup>4</sup> This tunability was achieved by employing a negative dielectrophoretic (DEP) virtual array of obstacles. In electrodeless or insulator-based DEP (iDEP) the varying electric field is present through the entire channel by insulating the microstructure between the electrodes using fabrication techniques such as soft lithography<sup>5</sup> or imprint lithography.<sup>6</sup> In this way the fabrication complexities involved with microelectrodes and other limitations commonly encountered in the presence of electrodes are avoided. Besides by using iDEP the device can be operated at DC fields as well as low frequencies without the need to be concerned about causing electrolysis.<sup>7</sup> In 2003, Cummings et al. investigated the effect of iDEP in continuous separation of particles through an array of insulating obstacles in two separate studies.<sup>8,9</sup> It was concluded that using DC fields, the particles flow can be focused and the critical size can be tuned in the range of 5–25 μm for 200 nm particles. In 2009 Beech et al. introduced a method called D-DLD where DEP and DLD are integrated together.<sup>10</sup> The particle separation behavior of the device was investigated using AC fields at low frequencies and it was shown that the critical size can be readily decreased by half or less. In a D-DLD the high resolution of DLD devices is combined with the tunability obtainable in DEP. Besides by changing the applied frequency different properties of the cells being investigated can be probed. In 2014 Kruger et al. investigated the possibility of separating red blood cells (RBC) in DLD devices in a simulation study and obtained positive results.<sup>11</sup> The displacement path taken by the RBCs was predicted in the particular DLD design.

<sup>a</sup> Division of Solid State Physics and NanoLund, Lund University, Professorgatan 1, 22363 Lund, Sweden. E-mail: jonas.tegenfeldt@ff.lth.se

<sup>b</sup> Division of Atomic Physic, Lund University, Professorgatan 1, 22363 Lund, Sweden.

In the present work we were using D-DLD to observe the behavior of RBCs at different applied AC voltages. We shall coin the term DEP-DLD instead to better describe the technique.

## 2. Theory

### Deterministic Lateral Displacement

The geometry in a deterministic lateral displacement (DLD) device, as shown in Fig. 1(a), consists of an array of bumpers with  $\lambda$  spacing between the centers, shifted laterally by a distance of  $\Delta\lambda = \lambda/N$ , where  $N$  is usually an integer number ( $2 \leq N \leq 100$ ).  $N$  is called the period of the array since the array repeats itself after  $N$  rows.

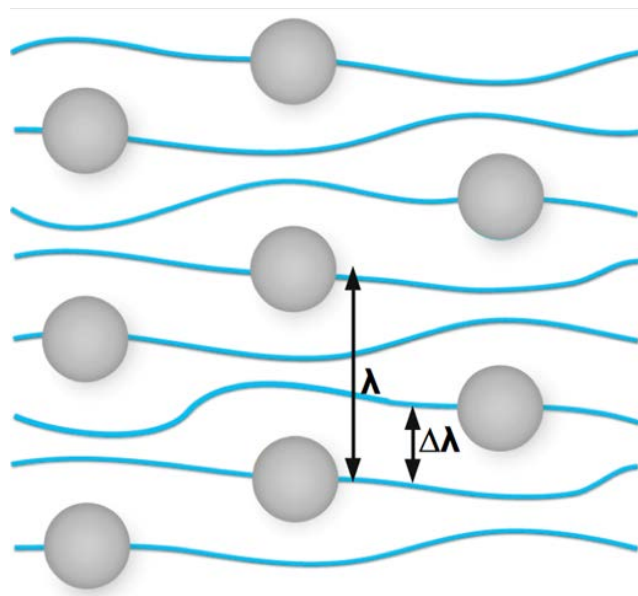


**Fig 1** A simplified bumper array with distance between two bumpers  $\lambda$ , row shift  $\Delta\lambda$  and period of  $N=3$ .

Laminar flow exists in micrometer sized fluidic channels of the DLD device. Depending on the forces applied on the particles, they follow the flow direction in straight or zigzag pattern. Particles which have the size less than a critical size value  $D_c$  move in zigzag pattern following the defined flow path while ones whose size  $D \geq D_c$  are transported in displacement mode. Fig. 2(a) shows the different trajectories of the particles depending on their size. The critical size (critical diameter) can be calculated as:

$$D_c = 2\alpha \frac{d}{N} \quad (1)$$

Where  $d$  is the distance between 2 posts and  $\alpha$  is correction term.

### Dielectrophoresis

Dielectrophoresis (DEP) is the phenomenon of motion of the particles subjected to a non-uniform electric field. The interaction of the field with the particle's dipole moment exerts a force on the particle. The force magnitude is uneven in different parts of the particle and this imbalance causes the

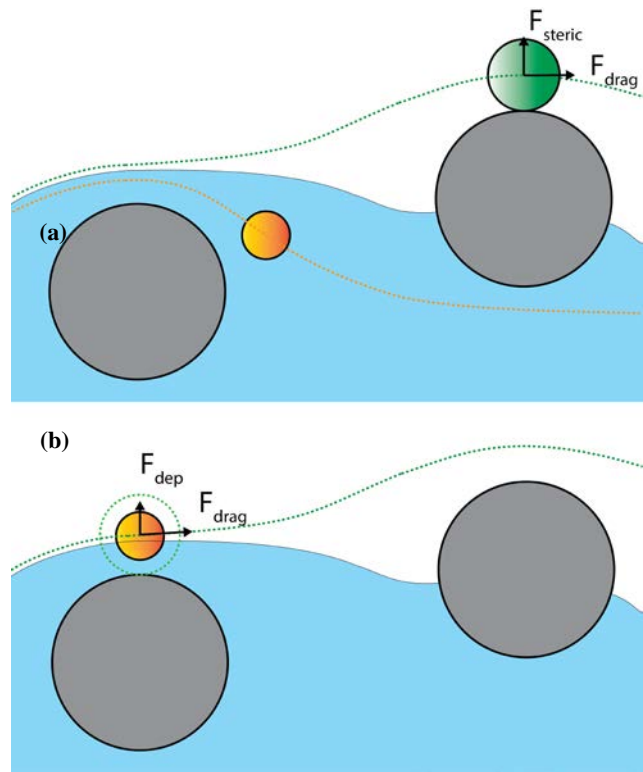


**Fig 2** (a) Trajectories of particles in a DLD device. The orange particle, which is smaller than the critical size, follows the stream while the big green particle “bumps” into the posts and switches to another stream. (b) Trajectories of a particle in a DEP-DLD device. Although it is smaller than the critical size, the dielectrophoretic force makes it appear larger and moves in displacement mode.

particle to move.<sup>12</sup> The force magnitude and direction are dependent on the particles' geometry (size and shape) and electrical properties of the particles and the buffer they are suspended in. This property can be employed in microfluidic separation and sorting techniques, in particular DLD.

In the electrodeless DEP approach we used in this project, the voltage is applied across the length of the device. Due to the presence of the PDMS posts inside the channel, the electric field is distorted around the posts. In particular, the maxima of electrical field are at the sides of the post which have tangents parallel to the flow direction. Fig. 2(b) illustrates the case the particle experiences negative DEP – it moves away from the particular post. In other words although the particle is smaller than the critical diameter, it behaves like a larger particle and gets deviated from the flow stream it originally reside.

## 3. Experimental

### Device

We used soft-lithography to make poly-(dimethylsiloxane) (PDMS) on glass device for our experiments. The detailed procedure can be found on the paper by Holm, Beech *et. al.*<sup>13</sup> We modified the design by Stefan Holm for sorting blood and *Trypanosoma cyclops*<sup>13</sup> to run our DEP-DLD experiments with red blood cells. The layout of the original design is shown in Fig. 3(a). In order to achieve high electric field, we shortened the device by cutting it in half and pinched the outlet hole near the cut line.

The complete device after tubing is illustrated in Fig. 3(b). The device has four reservoirs: two buffer reservoirs and a sample reservoir (on top of the figure) and an outlet reservoir (at the bottom of the figure). The four blue cylinders showed in the figures are part of the tubes connecting to the pressure pump and the four small wires are platinum electrodes.

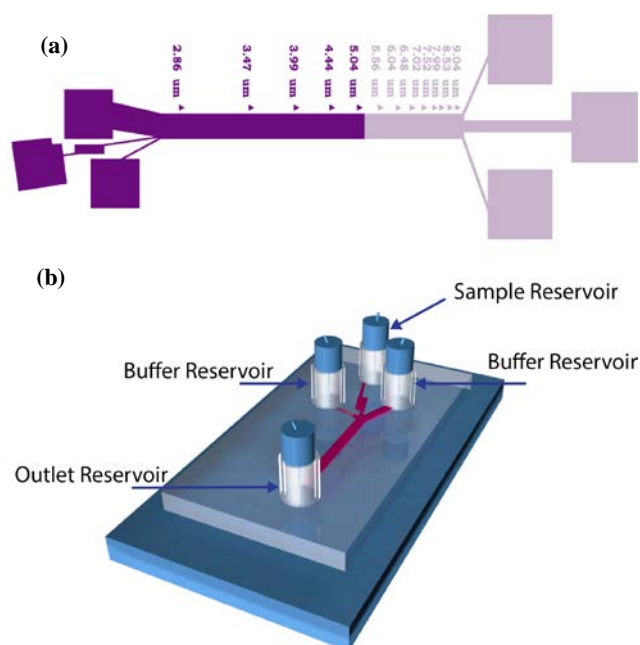


**Fig 3** (a) The DEP-DLD device modified from Holm's *Trypanosoma* design, the blurred half was cut out to shorten device length. (b) 3D model of the complete device.

### Equipment

The transportation of blood sample and buffer inside the PDMS device was driven by pressure gradient. Pressure at the sample reservoir and the two buffer reservoirs was regulated by an over-pressure pump (MFCS-4C, Fluigent, Paris, France) via three plastic tubes and connectors (Fig. 4). The pump maintained a stable pressure difference in the range of 0 – 60 mBar between the sample/buffer reservoirs and the outlet reservoir, which was left open to atmospheric pressure. To supply a high-voltage bias across the channel of the device, we used a function generator (33120A, Hewlett Packard, Palo Alto, CA, USA) together with a 100-time amplifier (BOP 1000M, Kepco, Flushing, NY, USA), yielding a sinusoidal AC voltage of up to 1000 Vpp. One terminal of the voltage source was connected to the two platinum electrodes immersed into the buffer at the buffer reservoirs and the other terminal was attached to the platinum electrode embedded into the buffer at the outlet reservoir. Since the cross-section of the buffer/outlet tubes is much larger than that of the fluidic channel, the electrical impedance of these tubes is much lower than the channel impedance and the voltage difference provided by the voltage source is assumed to only be distributed across the channel. Blood cells in the device were imaged through an inverted microscope (Eclipse TE2000-U, Nikon Corporation, Tokyo, Japan); the images and movies of

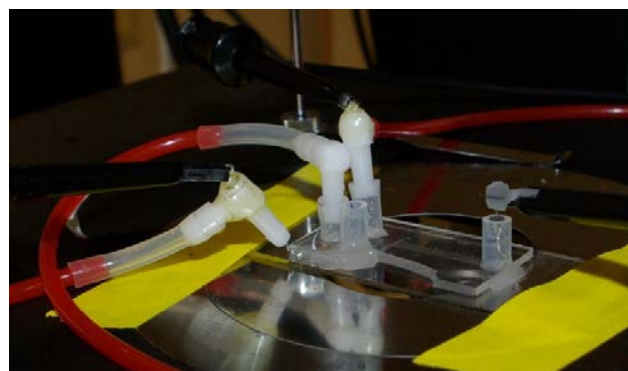


**Fig 4** The DEP-DLD device with microfluidic and electrical connections. The sample and buffer reservoirs (on the left of the device) were connected with an over-pressure pump by three plastic tubes; one of the tubes was unplugged for clarity. The buffer reservoirs and the outlet reservoir (on the right of the device) are connected to the AC voltage source through platinum electrodes attached to three electrical wire testing hooks.

the experiments are capture using a CMOS camera (Neo sCMOS, Andor Technology, Belfast, Northern Ireland).

### Sample preparation

The blood sample was extracted from healthy donors following a standard procedure. A sterile needle (Haemolance+ low flow, Haemedic, Sweden) is used to prick the donors' finger, the blood drop (10  $\mu$ l) is collected by a sterile pipette tip and then diluted in to 1000  $\mu$ l of autoMACS<sup>®</sup> running buffer (#130-091-221, Miltenyi Biotec, Bergisch Gladbach, Germany). The buffer (pH 7.2) contains phosphate buffered saline (PBS), bovine serum albumin (BSA), EDTA, and 0.09% sodium azide.

### Experimental procedure

Ten  $\mu$ l of diluted blood sample was added to the inlet reservoir and the buffer reservoirs were filled with autoMACS<sup>®</sup> running buffer. The outlet reservoir was also filled with the buffer to allow for electrical conduction. The experiment could be run with or without electrical voltage. Movies were taken on over the device; however, to quantify the displacement and effective size of the red blood cells, we focused on a small region near the outlet reservoir, which has the nominal critical size of 5.04  $\mu$ m (Fig. 5(a)). The AC voltage was ramped up from 0 V to 1000 Vpp, with the resolution of 200 Vpp. For each voltage value, we captured a corresponding microscopic movie. In each movie, we counted the number of RBCs passing through every gap between nearby posts of a chosen row. The cell counts are normalized and plotted as a function of the displacement.

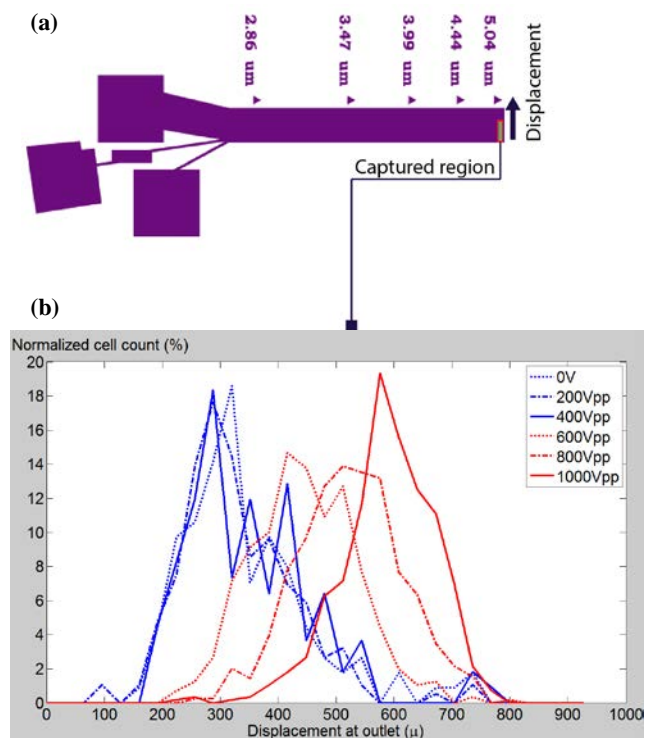


**Fig. 5** (a) The captured region where displacement of RBCs were analyzed. (b) Distribution of RBCs at the captured position. The graph shows cell count value at each displacement position along the chosen row for counting. There are six curves corresponding to six AC voltage values used in our experiments.

## 4. Results and Discussion

### Orientation of red blood cells in DEP-DLD device

RBCs have the shape of a biconcave disk, with diameter of around 6 – 8  $\mu\text{m}$  and thickness of around 2 – 2.5  $\mu\text{m}$ . Due to this specific geometry, orientation of the cells in a normal DLD device would change dependent on the fluid stream they resides in. When RBCs travel in a straight channel or in the middle of two bumpers, they align horizontally like Frisbees flying in mid-air. Looking at a microscopic image taken from the top of the device, one sees the cells as circles. However, when the RBCs switch to the fluid streams near a post, they tend to seek high contact area with the post and orient vertically like bicycle tires. From the top of the device, one sees the cells as thin, rounded rectangles (Fig. 6 (a) and Movie 1). This phenomenon dictates the effective size of the cells in a DLD device, making them appear as small as their thickness.<sup>13</sup>

When there was a decent electric field gradient distributed across the device, the mentioned vertical orientation of the RBCs when they move near the posts was overridden. As can be seen in Fig. 6(b) and Movie 2, the cells appeared consistently as Frisbees when they flowed in the bumper array, disregarding their position with respect to posts. The effective size of the cells is near their diameter.

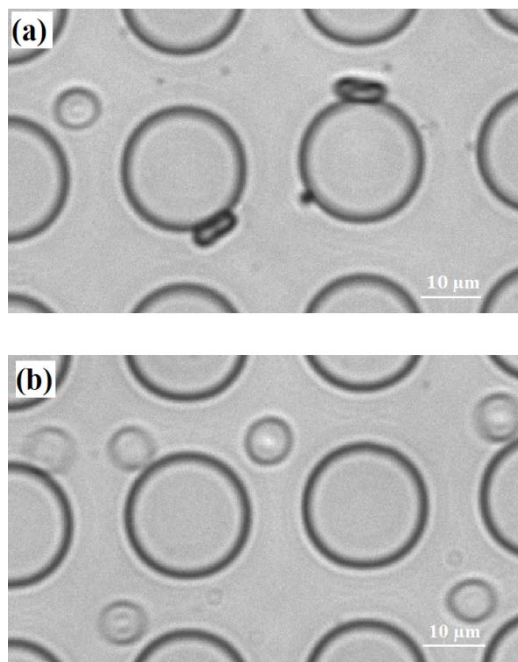


**Fig. 6** Orientation of red blood cells in a DLD device. (a) In the absence of an AC field ( $E = 0$ ), there are two types of orientation of RBCs depending on their positions with respect to a post. (b) When electric field was turned on ( $V = 1000$  Vpp,  $|E| \approx 177$  V<sub>RMS</sub>/cm), RBCs orient horizontally like Frisbees flying in mid-air, disregarding the fluid stream they were in.

### Distribution of red blood cells near the outlet reservoir

To quantify the dielectrophoretic effect on RBCs in DEP-DLD devices, we analyzed the displacement of the cells at a region near the outlet. Fig. 5(b) shows the distribution of RBCs measured at the end of our device. There are six curves corresponding to six AC voltage amplitudes we used, ranging from 0 to 1000 Vpp. As can be seen from the figure, when the applied voltage increased to 600 Vpp, the displacement of the RBCs started to change. This can be explained by the change in their orientation under dielectrophoretic effect, making them appear larger when in contact with a post and have the tendency to move in displacement mode throughout the channel.

### Effective size of RBCs in DEP-DLD

The bell-shaped curves in Fig. 5(b) can be fitted into normal distribution to estimate the effective size of RBCs in a DEP-DLD device. This work can be performed using the Curve Fitting application of MATLAB R2014a (The MathWorks, Natick, MA, USA). Fig. 7 shows the fitted data. The blue diamond marks represent the mean displacement of RBCs at each voltage value and the error bars correspond to one standard deviation. We also add the dotted lines noted with critical diameter values to help estimate the effective size of the cells in our device. For example, by looking at the graph one can see that when a voltage of 600 Vpp was applied, RBCs behave as spheres of diameters in the range between 3.47  $\mu\text{m}$  and 3.99  $\mu\text{m}$ .

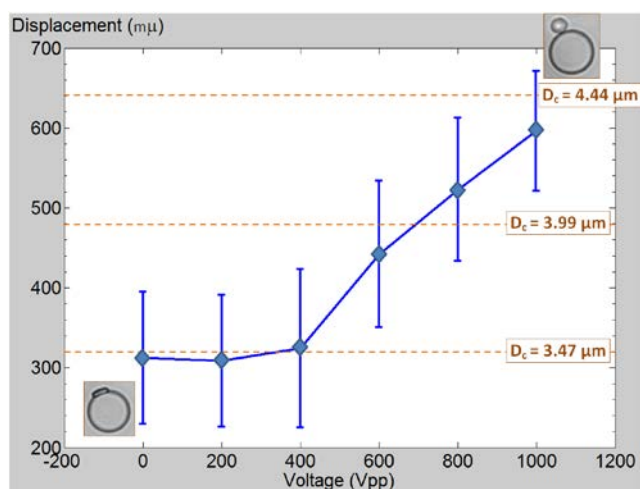


**Fig. 7** The displacement of RBCs as a function of applied voltage, assuming they have normal distribution. The dotted lines marked with critical diameter values are included to help estimate the effective size of the cells in our device.

In Fig. 7, one can see that the error bars are considerably large when comparing to the mean values. There are three possible factors causing this phenomenon. First, the RBCs already have their own size distribution, both in diameter and thickness. Second, the master we used to make PDMS device has some defects that make some posts disappear inside the device's channel and affect the flow profile. Finally, as can be seen from Movie 3, the orientation of RBCs while moving in the bumper arrays is quite stochastic. In particular, besides vertical and horizontal orientations they may also have inclined orientation that makes their effective size lies in the range between their thickness and their diameter. We believe that the third effect contributes the most to the errors seen in Fig. 7.

It should be noted that although the biggest size shown in Fig. 7 is 4.44  $\mu\text{m}$ , it does not reflect the actual diameter of the RBCs. The reason for this is that we only use half of the device, which has highest critical size value of 5.04  $\mu\text{m}$ , meaning that even if the cells were as large as 8  $\mu\text{m}$ , they would be still displaced to the same position as the ones having the diameter of 5.04  $\mu\text{m}$ . This drawback of the device can be avoided by a new DEP-DLD design that is more suitable for RBCs.

## 5. Conclusion and outlook

In this project, we have shown the effect of dielectrophoresis on orientation of RBCs in DLD devices. This property can be used as a tool to tune the effective size of RBCs by a factor of 1.5 (from below 3.47  $\mu\text{m}$  to 4.44  $\mu\text{m}$  in our work) or, even better, of three with more suitable design, keeping in mind that the diameter of the cells can be three times as large as their thickness. This phenomenon can open a wide range of applications in sorting RBCs from other kinds of cells and pathogens, thanks to the unique geometric of the anucleate RBCs.

There is plenty of room for future work. Due to limited time,

we were not able to carry out modelling and simulation of RBCs in the devices, which can help gain more insight into the mechanism behind the DEP effect on orientation of RBCs. The buffer we used in this work is isotonic; one can possibly treat RBCs with hypotonic buffer to make them more spherical, carry on similar experiments, and compare with our results to see whether the DEP force or torque (orientation change) is more pronounced. The device we used in this work is originally designed for morphology sorting. By designing a more suitable device for DEP-DLD, one can obtain more precise and promising data on the effective size of RBCs and possibly, applying DEP to separate RBCs from other kind of cells like breast cancer cell MCF-7 or *Trypanosoma cyclops*.

## Acknowledgement

The experiments in this work was performed at and supported by prof. Jonas Tegenfeldt's labs at Division of Solid State Physics, Department of Physics, Lund University.

## References

- 1 J. Guck, S. Schinkinger, B. Lincoln, F. Wottawah, S. Ebert, M. Romeyke, D. Lenz, H. M. Erickson, R. Ananthakrishnan, D. Mitchell, J. Käs, S. Ulvick and C. Bilby, *Biophys. J.*, 2005, **88**, 3689–3698.
- 2 S. Suresh, J. Spatz, J. P. Mills, a. Micoulet, M. Dao, C. T. Lim, M. Beil and T. Seufferlein, *Acta Biomater.*, 2005, **1**, 15–30.
- 3 L. R. Huang, E. C. Cox, R. H. Austin and J. C. Sturm, *Science*, 2004, **304**, 987–90.
- 4 S. Chang and Y.-H. Cho, *Lab Chip*, 2008, **8**, 1930–6.
- 5 Y. N. Xia and G. M. Whitesides, *Annu. Rev. Mater. Sci.*, 1998, **37**, 551–575.
- 6 S. Chou, P. Krauss and P. Renstrom, *Appl. Phys. Lett.*, 1995, **67**, 3114.
- 7 X. Xing, M. Zhang and L. Yobas, *J. Microelectromechanical Syst.*, 2013, **22**, 363–371.
- 8 E. B. Cummings, *IEEE Eng. Med. Biol. Mag.*, 2003, **22**, 75–84.
- 9 E. B. Cummings and A. K. Singh, *Anal. Chem.*, 2003, **75**, 4724–4731.
- 10 J. Beech, P. Jönsson and J. Tegenfeldt, *Lab Chip*, 2009, **9**, 2698–2706.
- 11 T. Krueger, D. Holmes and P. Coveney, *arXiv Prepr. arXiv1406.1877*, 2014, **054114**, 1–10.
- 12 R. Pethig, *Biomicrofluidics*, 2010, **4**.
- 13 S. H. Holm, J. P. Beech, M. P. Barrett and J. O. Tegenfeldt, *Lab Chip*, 2011, **11**, 1326–1332.

Cite this: DOI: 10.1039/xxxxxxxxxx

## Sorting bacteria by chain length<sup>†</sup>

Jason P. Beech,<sup>a</sup> Bao D. Ho,<sup>a</sup> Genevieve Garriss,<sup>b</sup> Vitor Oliveira,<sup>b</sup> Birgitta Henriques Normark,<sup>b</sup> and Jonas O. Tegenfeldt,<sup>\*a</sup>Received Date  
Accepted Date

DOI: 10.1039/xxxxxxxxxx

www.rsc.org/journalname

We show that different chain lengths of *Streptococcus pneumoniae* can be sorted using Deterministic Lateral Displacement microfluidic devices. In different outlets of the device, we were able to enrich either single cocci or chains with high purity. Also, we present a high throughput device capable of sorting out a million particles per minute, suitable for standard RNA analysis for bacteria.

### 1 Introduction

Cell separation is vital to many biomedical applications, especially diagnostics, therapeutics, and cell biology. Bench top cell sorting methods, including continuous flow cytometry, fluorescence-activated cell sorting (FACS), and magnetic-activated cell sorting (MACS)<sup>1</sup> have been commonly used by biomedical experts and technicians to sort a wide variety of cells at high throughput. Nevertheless, there are several disadvantages when using conventional cell sorting techniques: they require user specialization and training; the initial costs, operating costs, and reagent costs are high; and antibodies and fluorophores labeling may alter the functions of cells. There has been a search for simple, low cost, and reagent-free alternative cell sorting methods using microfluidic technology. Instead of employing chemical labels or tags to identify cells of interest, *label-free cell sorting* methods exploits intrinsic physical properties of cells, including but not limiting to size, shape, deformability, compressibility, density, dielectric properties, surface charge, et cetera, to fractionate cells.

*Deterministic Later Displacement* (DLD) is a label-free sorting approach, which sorts particles based on size<sup>2</sup>. Since 2004, DLD has been used to sort WBC from RBC and plasma<sup>3, 4, 5</sup>, separate circulating moving cells from blood<sup>6, 7</sup> or isolate trypanosome from blood<sup>8, 9</sup>. While bacteria are important pathogenic cells and their sizes range (one to several microns) are relevant for sorting using DLD, this possibility has not been exploited, with only an exception of a short note in an article by Zeming et. al.<sup>10</sup>, where the authors briefly tested the effects of I-shaped pillars DLD and found that it was effective in the separation of the *Escherichia coli* bacteria. Therefore, it is a natural and tempting yet unex-

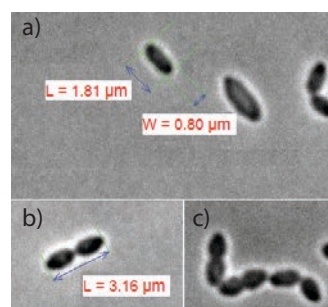


**Fig. 1** *Streptococcus pneumoniae* with three different morphologies: (a) singles, (b) diplococci and (c) chains

plored topic in the field of microfluidic separation.

Our attention directs toward *Streptococcus pneumoniae*, a Gram-positive member of the genus *Streptococcus*. A population of *S. pneumoniae* is heterogeneous in morphology: they can appear in the form of single bacteria, chains of two (diplococci) or chains of more than two bacteria, which can be seen in Figure 1. Our goal is to separate those different morphologies of *S. pneumoniae* using DLD because of several medical and technological grounds. Firstly, *S. pneumoniae* is a major cause of pneumonia in humans which leads to around one million deaths worldwide annually, and thus, is the subject of many humoral immunity studies. Secondly, single bacteria and chains show different pathogenic properties: it is believed that longer chains can adhere more to epithelial cells in the lung while shorter chains and singles are more able to evade the immune system<sup>11, 12</sup>. Therefore, there is an interest in sorting these different morphologies.

In this work, we perform sorting of *S. pneumoniae* by chain length using DLD. The difference in length causes different hydrodynamic behaviors of long and short chains in a DLD device, suggesting the possibility of separating them with the device. With a device having the critical diameter approximates to the size of a single coccus, we were able to enrich single cocci in some outlets

<sup>a</sup> Division of Solid State Physics and NanoLund, Lund University, Professorgatan 1, 22363 Lund, Sweden. E-mail: jonas.tegenfeldt@ftf.lth.se

<sup>b</sup> Department of Microbiology, Tumor and Cell Biology, Nobels väg 16, KI Solna Campus Karolinska Institutet, Box 280, 17177 Stockholm, Sweden

<sup>†</sup> Electronic Supplementary Information (ESI) available: [details of any supplementary information available should be included here]. See DOI: 10.1039/b000000x/

and chains of bacteria in the other ones. A high throughput device capable of sorting roughly a million of particles per minute was also designed, fabricated, and tested with polystyrene beads.

## 2 Theory of DLD

The mechanism of DLD has been clearly explained by Huang et al.<sup>2</sup>. We illustrate this mechanism in Figure 2. We call a line of pillars perpendicular to the flow direction a *row*; the next row along the flow direction is shifted up a small distance with respect to the previous row. This asymmetric arrangement causes the flow bifurcated when it encounters a pillar, as can be seen at the bottom of Figure 2: a small stream of the flow, highlighted in tint color, goes around and under the pillar on the bottom right corner while the rest keeps going straight above that pillar. If the centre of mass of the particle resides within the small stream (the green particle), the particle will also go around and under the pillar while the bigger one (the red particle) whose centre of mass does not fit into the tint stream will travel above the pillar. This separation is accumulated along the device causing different trajectories of the green and the red particles: one going zig-zagging with zero net displacement in the perpendicular direction to the flow while the other being pushed continuously and ending up being *deterministically lateral displaced* at the end of the array.

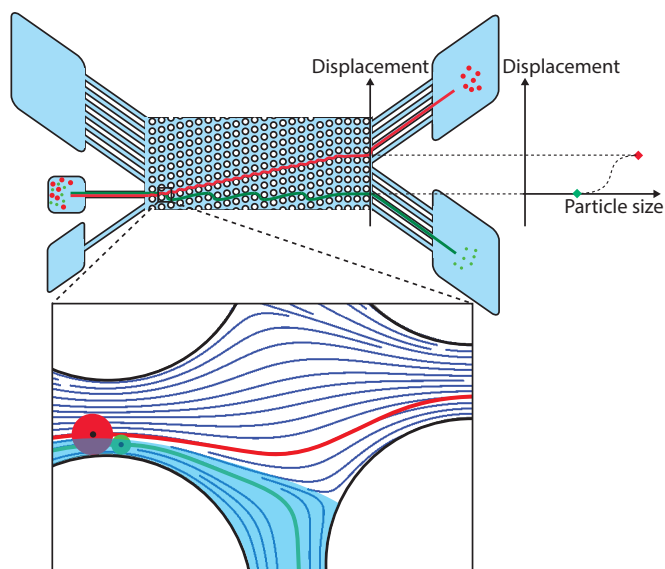


**Fig. 2** The principle of DLD. The device was shown on the top, capable of sorting big (red) and small (green) particle in two populations. The inset at the bottom illustrates the mechanism.

## 3 Experimental

### 3.1 Fractionation of *Streptococcus pneumoniae* by chain length

The device used to sort *Streptococcus pneumoniae* according to different chain length is shown in Figure 3. The pillars and microfluidic channels were defined using the standard PDMS soft lithography method<sup>13</sup>. The device has one sample inlet, one buffer inlet, and five outlets corresponding to five ranges of displacement of particles. The critical diameter is estimated to be  $1.24 \mu\text{m}$ , using

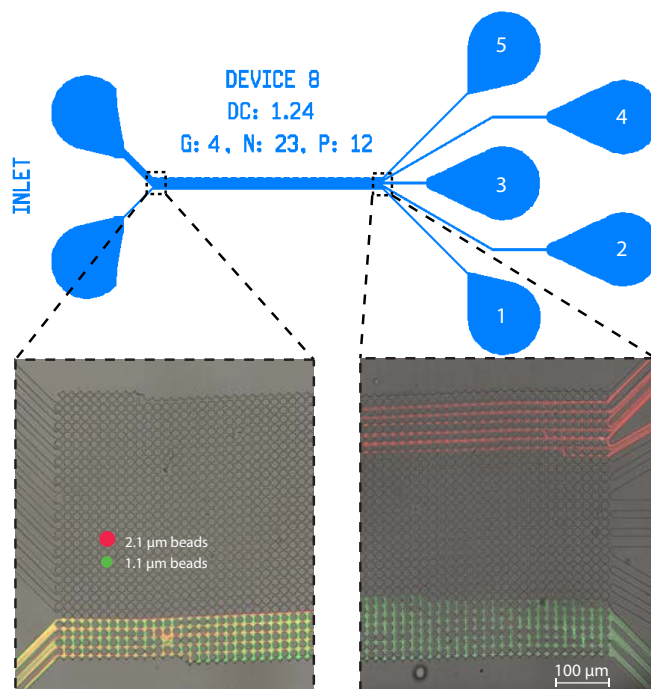
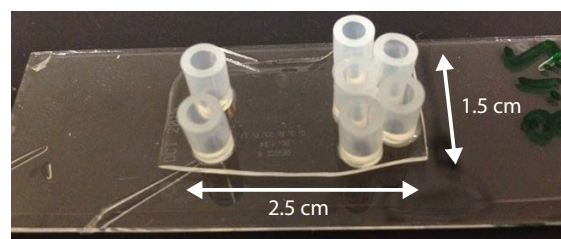


**Fig. 3** A DLD device with the critical diameter of approximately  $1.24 \mu\text{m}$ . The device was able to separate a mixture of  $1.1 \mu\text{m}$  and  $2.1 \mu\text{m}$  polystyrene beads.

the empirical equation 1, proposed by John Davis<sup>14</sup> (page 24):

$$D_C = 1.4GN^{-0.48} \quad (1)$$

Where  $D_C$  is the critical diameter,  $G$  is the gap width, and  $N$  is the period of the array.

The critical diameter was verified with polystyrene beads of two different sizes:  $1.1 \mu\text{m}$  and  $2.1 \mu\text{m}$ .

The device was then used to sort bacteria. To minimize sticking, the device (PDMS stamp) was bonded on a PDMS-coated glass slide, then coated with PLL-PEG (0.2% (w/v) PLL(20) – g[3.5] – PEG(2)) in deionized water and allowed to rest for at least 20 minutes before flushing with deionized water for another 20 minutes. *S. pneumoniae* R6-gfp, a non-pathogenic, green fluorescence strain, was selected for the experiments. The bacteria were suspended in PBS + 1% BSA buffer at final optical density  $OD_{620\text{nm}} \approx 1$ . The bacteria have three different morphologies, as shown in Figure 1; there are fewer chains than singles or diplococci. Flow was generated in the device using an overpressure of 60 mBar applied at the inlets with an MFCS-4C pressure controller (Fluigent, Paris, France). After sorting, the different morphologies of bacteria in each reservoir were blind-counted to

avoid bias.

### 3.2 Highthroughput sorting device

Results in Section 4.1 prove that separation of different morphologies of *S. pneumoniae* is feasible with DLD. The next step is to scale up the number of bacteria sorted. A highthroughput device is desirable due to two main reasons:

- To study a population of single cocci or a population of chains using RNA extraction and analysis, a large quantity of bacteria needs to be sorted, which is around 1 – 10 million colony-forming unit (CFU), within a time scale shorter than the bacteria's doubling time, which is around 20 – 30 minutes. This is far beyond the capability of the device presented in Section 3.1.
- Furthermore, due to the inherent overlapping between the size distribution of singles and diplos and between chains and diplos, to obtain sufficiently pure population of single cocci, the critical diameter needs to be sufficiently small so that most of, if not all, diplo cocci are filtered out. Similar argument applies to sorting chains, but in this case the critical diameter should be large enough to remove diplo cocci from longer chains. This requirement on purity further reduces the quantity of bacteria can be collected after sorting.

To make a high throughput device, we placed 64 DLD arrays in parallel on the same chip (Figure 4), which helps scale the throughput up to 64 times. The device was also deeper than the device described in Subsection 3.1 ( $15\ \mu\text{m}$  versus  $10\ \mu\text{m}$ ) and the post diameter to gap width ratio is smaller, for the same purpose of increasing the throughput. The device has one big inlet, one big product outlet, and 64 small waste outlets, which were not joined and collected. To run the device, a mixture of big and small particles suspended in a liquid medium was loaded into the inlet and an over pressure was applied there to generate a pressure driven flow across the DLD arrays towards the outlets. The liquid in the inlet was divided equally into 64 streams, running into each array. In this specific device, the arrays were intended to enrich single cocci only and remove all diplo cocci and chains, thus it was designed to have the critical diameter of  $1.1\ \mu\text{m}$ , which is smaller than that of the device presented in the Subsection 3.1. Two sizes of polystyrenes beads,  $1.1\ \mu\text{m}$  and  $2.1\ \mu\text{m}$ , with different fluorescence colors were mixed and run through the high throughput device. In each array, bigger particles (red) were supposed to be displaced to one side while small particles (green) were allowed to travel zig-zagging uniformly across the width of an array; thus, a pure population of small particles can be collected. Figure 4c) shows such two arrays, the one on the right was designed to be the mirrored image of the one on the left, making it easier to join the two streams of small particles into the product outlet.

## 4 Results and discussion

### 4.1 Fractionation of *Streptococcus pneumoniae* by chain length

For characterization purpose, we were able to sort the mixture of  $1.1\ \mu\text{m}$  and  $2.1\ \mu\text{m}$  polystyrene beads into two populations using

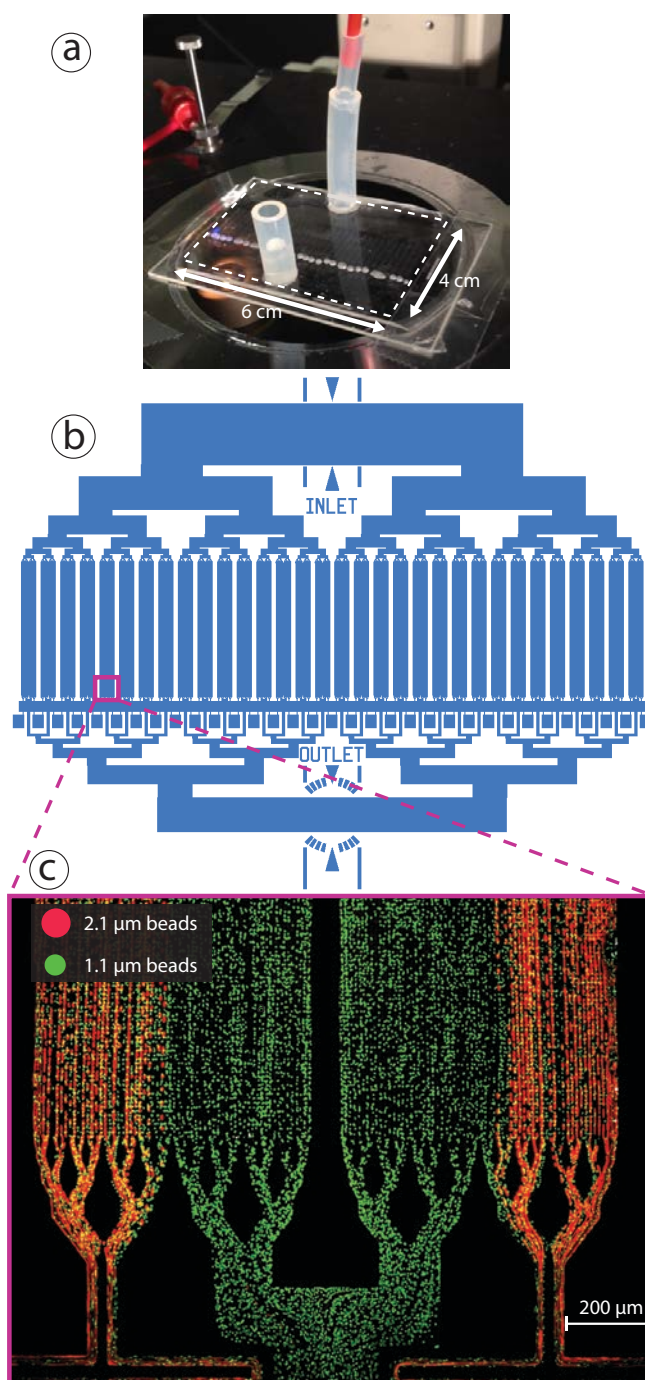


**Fig. 4** The high throughput device. a) The device on a microscope stage, in action. b) The design of the device. c) The device was characterized with beads of two different sizes:  $1.1\ \mu\text{m}$  and  $2.1\ \mu\text{m}$ , with an over pressure of 200 mBar. The image was a superimposed image of ten consecutive frames, taken at 25 fps.

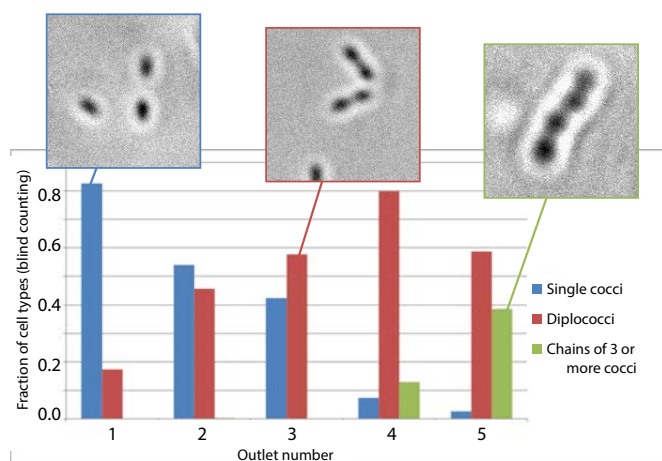


**Fig. 5** Distribution of different morphologies of *S. pneumoniae R6-gfp* at five outlets of the device described in Figure 3. The height of the columns represents the relative number of different morphologies in each reservoir (meaning that the columns in each reservoir add up to unity and comparison between columns of the same color in two different reservoirs is irrelevant).

the device of five outlets whose  $D_C$  is estimated to be  $1.24 \mu\text{m}$ . As shown in the insets of Figure 3, the mixture of beads were separated apart: the smaller beads ( $1.1 \mu\text{m}$ ) were collected into outlet 1 and the bigger ones were captured in outlet 5. This confirmed that the critical diameter of the device is between  $1.1 \mu\text{m}$  and  $2.1 \mu\text{m}$ .

When using the same device to sort bacteria, the bacteria's distribution inside each outlet was plotted in the graph of Figure 5, where the outlets are numbered in increased displacement tendency, as already labeled in Figure 3.

The graph shows enrichment of chains in more displacing reservoirs (4 and 5) and singles in more zig-zagging reservoirs (1, 2 and 3). Further more, there is almost no chains in the more zig-zagging reservoirs (1, 2 and 3) and very few percentage of singles in the more displacing reservoirs (4 and 5), proving that separating single bacteria and chains is completely feasible with this device. However, the appearance of diplococci in almost every outlet makes it difficult to achieve high purity of singles or chains sorted. This limitation can be resolved by reducing the critical diameter to collect purer population of singles in reservoir 1 or increasing the critical diameter to collect purer population of chains in reservoir 5 at the cost of getting fewer bacteria in each population.

The fact that diplococci were found at every outlet can be explained by the variation in size of diplococci, which is illustrated in Figure 6. In Figure 1, close to the top right corner, it is also apparent that single cocci are also diverse in size and can be as big as small diplococci.

Dynamics of *S. pneumoniae* in the DLD device was shown in Figure 7. High frame rate, bright field (no fluorescence), close-up videos were taken to capture the trajectories of different morphologies of the bacteria in the device. The images in Figure 7 were extracted from the videos using ImageJ. The image processing procedure is as follows:

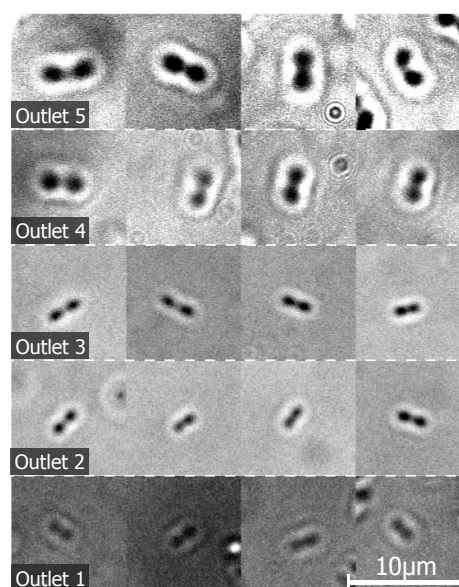


**Fig. 6** Diplococci having different sizes in different outlets of the DLD device. All images were taken at the same magnification.

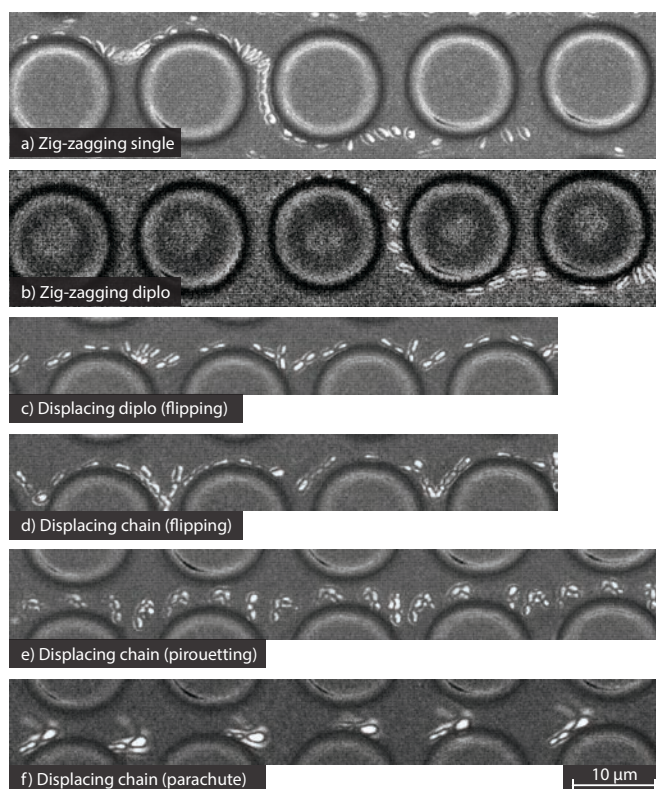


**Fig. 7** Dynamics of different morphologies of *S. pneumoniae R6-gfp* in DLD device. (a) A single coccus was transported in zig-zagging mode; (b) and (c) A diplo coccus may follow a zig-zagging mode or a flipping displacing mode, depending on its length; (d), (e), and (f) A chain can have different displacing mode, depending on how it bends.

i. The frames of a video were averaged to yield a background image.

ii. A new set of frames were generated by taking the difference of the original frames and the background. The new frames, after brightness and contrast were adjusted, would show bright bacteria on a relative dark background.

iii. A smaller set of frames were chosen among the frames in step ii and max intensity Z-stacking were performed to yield the images shown in Figure 7.

Figure 7b) and c) show the dependence of a diplo's trajectory on its length: while a short diplo coccus follows a zig-zagging trajectory like a single coccus, a sufficient long diplo would perform a flipping move from pillar to pillar and displayed displacing tendency. Figure 7d) illustrates similar displacing mode of a chain of six singles (although it looks more like a chain of three, it is actually a chain of six, which is visible from the original video). Figure 7e) and f) show two other displacing modes of chains, which are pirouetting (a bended chain rotating around its longer arm while moving between the pillars' gaps, although the rotating movement is not quite clear from the picture) and parachute (a chain bended like a boomerang while it moved between the pillars' gaps).

#### 4.2 Highthroughput sorting device

The result of running  $1.1\ \mu\text{m}$  and  $2.1\ \mu\text{m}$  beads in the high throughput device was shown at the bottom of Figure 4. Although the critical diameter of the device was estimated to be  $1.1\ \mu\text{m}$ , all the  $1.1\ \mu\text{m}$  beads were going zig-zagging, meaning that either the empirical formula 1 was not accurate in this case or there had been some deviation in the gap width between two neighboring pillars, due to errors introduced in the fabrication process. Nevertheless, all  $2.1\ \mu\text{m}$  beads were pushed to one side as expected, leaving only pure population of small beads being collected into the product outlet. The volumetric throughput when running at  $200\ \text{mBar}$  over pressure was  $43\ \mu\text{L}/\text{minutes}$  and the quantitative throughput into the product outlet is roughly  $25000\ \text{beads}/\text{second}$ . This means to obtain a million beads, the running time is only  $40\ \text{seconds}$ , which is a promisingly short running time, with regards to the bacteria doubling time of around  $20 - 30\ \text{minutes}$ . Nevertheless, it should be noticed that running biological sample in DLD device is prone to sticking and clogging problem. The next step would be running *S. pneumoniae* in this device and making efforts to minimize sticking and clogging problem to obtain desired quantity of bacteria for RNA analysis.

## 5 Conclusions and future work

We have, in this study, shown that separation of bacteria by chain length using DLD is feasible. With a device having critical diameter

close to the size of a single coccus, we were able to enrich single cocci in the most zig-zagging outlets of the device and chains in the most displaced ones.

A high throughput device was also designed, fabricated, and characterized with polystyrene beads, showing that obtaining millions of particles in minutes is a realistic goal. In a very near future, we will use the high throughput device to sort bacteria, together with optimizing the critical diameter so that pure single cocci or pure chains populations can be obtained in sufficient number for subsequent biomolecular analyses.

## References

- 1 D. R. Gossett, W. M. Weaver, A. J. Mach, S. C. Hur, H. T. Tse, W. Lee, H. Amini and D. Di Carlo, *Anal Bioanal Chem*, 2010, **397**, 3249–67.
- 2 L. R. Huang, E. C. Cox, R. H. Austin and J. C. Sturm, *Science*, 2004, **304**, 987–90.
- 3 J. A. Davis, D. W. Inglis, K. J. Morton, D. A. Lawrence, L. R. Huang, S. Y. Chou, J. C. Sturm and R. H. Austin, *Proc Natl Acad Sci U S A*, 2006, **103**, 14779–84.
- 4 S. Zheng, R. Yung, Y.-C. Tai and H. Kasdan, 18th IEEE International Conference on Micro Electro Mechanical Systems, 2005. MEMS 2005., 30 J, pp. 851–854.
- 5 N. Li, D. T. Kamei and C. M. Ho, 2007 2nd IEEE International Conference on Nano/Micro Engineered and Molecular Systems, 16-1, pp. 932–936.
- 6 K. Louthback, J. D'Silva, L. Liu, A. Wu, R. H. Austin and J. C. Sturm, *AIP Adv*, 2012, **2**, 42107.
- 7 Z. Liu, F. Huang, J. Du, W. Shu, H. Feng, X. Xu and Y. Chen, *Biomicrofluidics*, 2013, **7**, 11801.
- 8 S. H. Holm, J. P. Beech, M. P. Barrett and J. O. Tegenfeldt, *Lab Chip*, 2011, **11**, 1326–32.
- 9 S. H. Holm, J. P. Beech, M. P. Barrett and J. O. Tegenfeldt, *Anal. Methods*, 2016, **8**, 3291–3300.
- 10 K. K. Zeming, S. Ranjan and Y. Zhang, *Nat Commun*, 2013, **4**, 1625.
- 11 J. L. Rodriguez, A. B. Dalia and J. N. Weiser, *Infect Immun*, 2012, **80**, 3454–9.
- 12 A. B. Dalia and J. N. Weiser, *Cell Host Microbe*, 2011, **10**, 486–96.
- 13 Y. Xia and G. M. Whitesides, *Annual review of materials science*, 1998, **28**, 153–184.
- 14 J. A. Davis, *PhD thesis*, Princeton University, 2008.